Thermal Instability of Railways

Eduardo Nava

Dissertation presented to the School of Technology and Management of Bragança to obtain the Master's Degree in Industrial Engineering. Work developed during the double degree exchange program between the Polytechnic Institute of Bragança (IPB) and the Federal Technological University of Paraná (UTFPR).

Work oriented by:

Prof. Dr Paulo Piloto

Prof. Dr Manuel Minhoto

Prof. Dr Diego Rossetto

Bragança

2022-2023

ACKNOWLEDGMENTS

Firstly, I would like to thank my family, my mother Sirlei, my father Sérgio, and my sister Simone, who have always been by my side, supporting my decisions and providing me with the means to pursue dual degree studies. They have provided me with all the support and assistance I needed to achieve my goals. Without them, none of this would be possible.

I am grateful to God, whatever form He may take, for the opportunities I have had in life and the experiences I have gained throughout my journey. I thank Him for granting me good health, and prosperity, and surrounding me with incredible people who have been instrumental in shaping my character.

I extend my gratitude to my advisors, Professor Dr Manuel Minhoto, Dr Paulo Piloto, and Dr Diego Rossetto, for guiding me in this work and always being available to answer my questions and provide advice.

I would like to express my appreciation to the educational institutions, the Federal Technological University of Paraná (UTFPR) in Pato Branco and the Polytechnic Institute of Bragança (IPB), for providing me with the opportunity to study in another country and for supplying the necessary tools and educational infrastructure.

Lastly, I want to thank all my friends. They have helped me stay calm during turbulent and uncertain times. They have given me friendships that will last a lifetime and made the entire process of dual degree studies much easier.

AGRADECIMENTOS

Primeiramente gostaria de agradecer a minha família, minha mãe Sirlei, meu pai Sérgio e minha irmã Simone, que sempre estiveram ao meu lado, apoiando minhas decisões e me dando condições para viver o processo de dupla diplomação. Me proporcionaram todo o suporte e apoio para que eu alcance meus objetivos. Sem eles nada seria possível.

Agradeço a Deus, seja ele qual for, pelas oportunidades que tive na vida e pelas experiencias que tive durante toda minha caminhada. Por me proporcionar saúde, prosperidade e por me rodear de pessoas incríveis, que foram imprescindíveis na formação de meu caráter.

Agradeço aos meus orientadores, Professor Dr. Manuel Minhoto, Dr. Paulo Piloto e Dr. Diego Rossetto, por me guiarem neste trabalho e sempre estarem a disposição para sanar duvidas e me aconselhar.

Agradeço as instituições de ensino, Universidade Tecnológica Federal do Paraná (UTFPR) campus Pato Branco e Instituto Politécnico de Bragança (IPB) por proporcionarem a oportunidade de estudar em outro país e fornecerem as ferramentas e infraestrutura de ensino.

Por último gostaria de agradecer a todos os meus amigos. Eles me ajudaram a manter a calma em momentos turbulentos e de incertezas. Me proporcionaram amizades que levarei pra vida toda e tornaram todo o processo de dupla diplomação muito mais fácil.

ABSTRACT

The railway is a widely used mode of land transportation around the world. To ensure passenger comfort and safety, a specific structure is required, consisting of elements that are divided into infrastructure and superstructure. The superstructure encompasses the rails, sleepers, ballast, and fastening materials, which will be addressed in this study. The efficiency and safety of transporting people and goods on the railway depend largely on the behaviour of this superstructure. Under extreme environmental conditions, such as temperature fluctuations, there is a significant risk of thermal buckling of the rails, which can affect the behaviour of the other elements of the superstructure. This study aims to analyze how these various factors affect the occurrence of thermal buckling in railways. The research identifies rail misalignment and the quality of the ballast as the most influential factors in determining buckling temperatures. The study uses a numerical model, validated through experimental results, to conduct a parametric analysis. The parametric study identified ballast strength as the most critical parameter. When comparing the weak ballast condition (no crib ballast) to the complete and compacted ballast, an increase of up to 127% in buckling temperatures was observed. Additionally, it was observed that the initial rail imperfection significantly influences buckling temperatures. On the other hand, the other evaluated parameters such as rail profile and torsional stiffness had only a minimal influence on buckling temperatures.

Keywords: Thermal Buckling; Railways; Temperature

RESUMO

A ferrovia é um meio de transporte terrestre amplamente utilizado em todo o mundo. Para garantir o conforto e a segurança dos passageiros, é necessário ter uma estrutura específica, composta por elementos que são divididos em infraestrutura e superestrutura. A superestrutura abrange os trilhos, travessas, lastro e materiais de fixação, que serão abordados neste trabalho. A eficiência e segurança do transporte de pessoas e mercadorias na ferrovia dependem, em grande parte, do comportamento dessa superestrutura. Em condições ambientais extremas, como flutuações de temperatura, há um risco significativo de flambagem térmica dos trilhos, o que pode afetar o comportamento dos demais elementos da superestrutura. Este estudo tem como objetivo analisar como estes diversos fatores afetam a ocorrência de flambagem térmico em ferrovias. A pesquisa identifica o desalinhamento dos trilhos e a qualidade do lastro como os fatores mais influentes na determinação das temperaturas de flambagem. O estudo utiliza um modelo numérico, validado por meio de resultados experimentais, para realizar uma análise paramétrica. O estudo paramétrico identificou a resistência do lastro como o parâmetro mais crítico. Ao comparar a condição de lastro fraco (sem lastro entre travessas) com o lastro completo e compactado, foi observado um aumento de até 127% nas temperaturas de encurvamento. Além disso, foi observado que a imperfeição inicial do trilho tem grande influência nas temperaturas de flambagem. Por outro lado, os outros parâmetros avaliados tiveram apenas uma influência mínima nas temperaturas de flambagem.

Palavras-chave: Encurvamento Térmico; Ferrovias; Temperatura.

LIST OF FIGURES

LIST OF TABLES

LIST OF ABBREVIATIONS AND ACRONYMS

AREMA	American Railway Engineering and Maintenance-of-Way Association
GMNIA	Generalized Method of Neutral Incremental Analysis
VNTSC	Volpe National Transportation Systems Center
RMSE	Root mean square error
CWR	Continuous welded rail
UIC	International Union of Railway
FEA	Finite element analysis
IBE	Infinite boundary elements
STPT	Single tie push test
TPPT	Track panel push test
FRA	Federal railway administration
EXP	Experimental
NUM	Numerical simulation
ETA	Every tie anchored
EOTA	Every other tie anchored

LIST OF SYMBOLS

E	Elasticity Modulus
ε	Strain
σ_0	Yield Stress
ΔT	Temperature Increase
μ	Poisson's ratio
G	Shear Modulus
M	Torsional moment
F	Force
Θ	Rotational angle
σ	Displacement on the lateral direction
L_0	Imperfection length
λ	Slenderness ratio
I_{yy}	Moment of inertia about the y-axis
I_{zz}	Moment of inertia about the x-axis
n	Sample size
$\hat{y}_i$	Observed value for sample *i*
y_i	Predicted value by the model for sample *i*

TABLE OF CONTENTS

1. Introduction

1.1. Framework

Railway usage dates back to the seventeenth and eighteenth centuries. In its early days, railways were constructed using stone slabs or timber baulks and were initially pulled by horses. As the need arose to transport heavier loads, the wagons became increasingly heavier. Consequently, the initial railway infrastructure proved to be inefficient [1]. Evidence shows that the first railway infrastructures could be dated to the Roman and Greek ages, consisting of simple guidelines for carriages [2].

The implementation of continuous welded rail (CWR) on a global scale has been driven by advancements in railway technologies and the growing demand for safer and more comfortable railway systems. CWR outperforms traditional jointed rail tracks in various aspects such as speed, cost, noise, and vibrations. It enables smoother operations, requires less maintenance, reduces noise levels, and enhances passenger comfort, thus making it the preferred option for modern railways. [3].

As global temperatures rise and continuous welded rails become more prevalent, railways face an environment that is prone to buckling. This poses a safety risk as it can lead to derailments, forcing railway operators to implement operational stops and reduce speeds [4]. According to the UIC Safety Report 2022, in 2021, a total of 150 derailments were recorded in countries that participated in the report and provided data [5].

Railway thermal buckling occurs due to the combined effects of temperature fluctuations and structural constraints within the tracks. When the ambient temperature changes, CWR expand or contract accordingly, exerting stress on the track system that can lead to buckling.

This study aims to enhance our understanding of railway buckling by conducting a parametric analysis using Finite Element Analysis (FEA). The model developed for this analysis was validated by comparing it with previous experimental research, specifically focusing on scenarios without vertical loads. The study investigates various parameters, including rail profile, ballast resistance, fastener torsional stiffness, sleeper material, initial track misalignment, and track type (tangent and curved).

1.2. Research Objectives

The primary objective of this study is to analyse the impact of various parameters on rail buckling temperatures. To accomplish this, a Finite Element Analysis is performed, and the model is validated accordingly. Subsequently, numerous numerical simulations are carried out, where different parameters are varied, and the collected data is analyzed to assess the individual influence of each parameter.

1.3. Structure of Document

This work is structured in five chapters. The first chapter, the introduction, provides a brief overview of the history of railways, technological advancements, and the challenges encountered.

The second chapter consists of a literature review that defines the main elements of railways, explores the key parameters influencing static rail buckling, and examines previous studies on rail buckling, including experimental tests, finite element analysis, and analytical models.

The third chapter focuses on the methodology employed in this work. It begins by defining the elements used in the numerical model, followed by model validation, and concludes with a parametric study.

The fourth and fifth chapters present the results and conclusions, respectively. These chapters showcase the findings from the parametric study and the data analysis. Additionally, the main conclusions drawn from this work are outlined.

2. Literature Review

2.1. Railway Elements

The performance of railway tracks is the result of a complex interaction of various elements and layers of the system, in response to the demands imposed by rolling stock under different environmental conditions. Each part of the structural system must properly fulfil its function for the operation to be appropriate, guaranteeing that the whole is resilient, and stable, and prevents permanent deformations in the rails and wear of the components [6]. Figure 2.1 shows the division of the rail elements.

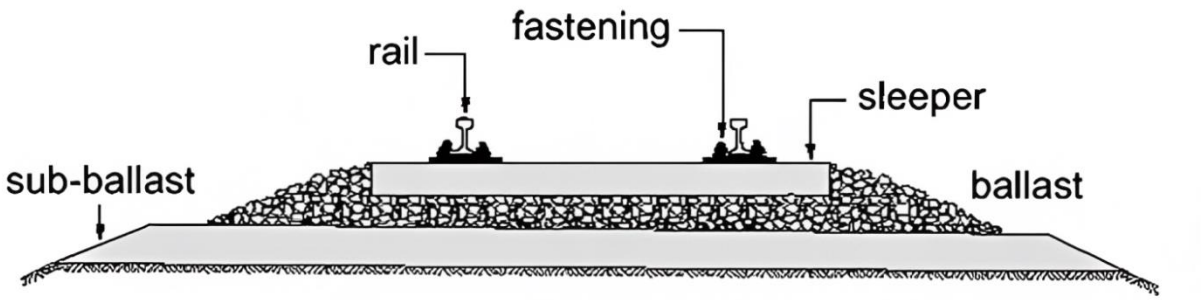

Figure 2.1 - Railway Superstructure [7]

To comprehend the behaviour of railway structures, it is crucial to highlight the principal sources of loads acting upon the system. The rolling stock stands as the primary origin of these loads, which are imposed upon the rail structure. It is widely adopted in most railway systems to employ twin rails and flanged wheels, as depicted in Figure 2.2. Due to the configuration of the wheels,

the forces are transmitted to the rail structure through three distinct mechanisms: direct compression exerted on the top surface of the rail by the wheel tire, lateral pressure applied by the flange, or friction along the longitudinal axis. [1].

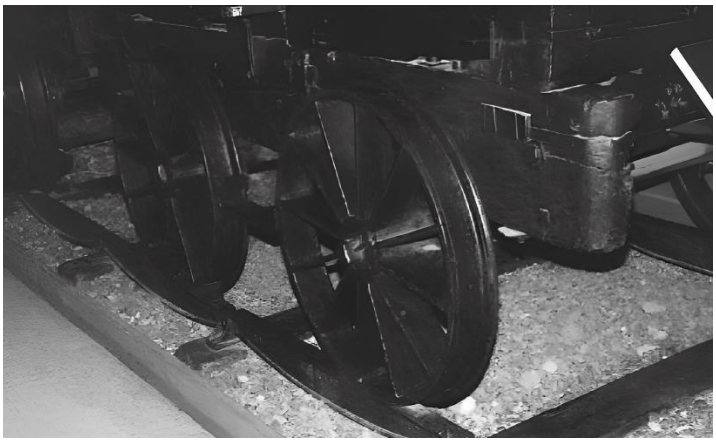

Figure 2.2 - Early flanged wheels [1]

With the development of new technologies, such as new rail profiles, different sleeper's materials and shape as well as the ability to provide more resistance within the ballast, railways could support the cruise of faster and more comfortable train cars.

2.1.1. Rails

Before the use of steel rails, it was common on the railways to have cast iron rails. The introduction of stiff iron rails and hard iron wheels with low rolling resistance facilitated the transportation of large loads [8]. This technological limitation restrained the speed limits of railway usage. Subsequently, steel emerged as a substitute material for both rails and rolling stock components.

Steel rails are a fundamental component of modern railways, manufactured to possess the necessary qualities of strength, fatigue endurance, and resistance to wear and corrosion. These rails are specifically rolled from steel to meet the precise requirements of railway track systems [1].

The presence of rail expansion joints was necessitated due to the thermal expansion of rail materials, imposing limitations on rail lengths. Consequently, these joints resulted in a less comfortable travelling experience, characterized by a noticeable unevenness or bumpiness during rail trips that also limited the safe speed that trains could travel. Continuous welded rail (CWR) was introduced as a solution to eliminate rail joints. This innovation offered several advantages, including decreased wear on rolling stock, minimized subgrade damage, extended rail lifespan, and reduced maintenance costs [9]. One of the problems on the CWR train tracks is increased compressive stresses in the rails due to temperature fluctuations and lack of rail joints.

Different rail geometries have been adopted through the years. The bullhead (Also known as double head profile) exhibits a rounded top with a flat bottom, closely resembling the contour of a bull's head (Figure 2.3.a). In the past, bullhead rails were frequently employed in antiquated railway networks. Nonetheless, their usage has significantly decreased over time, and they have been predominantly substituted by flat-bottomed rails in contemporary railway systems. The flat-bottomed profile, also called the Vignoles profile, is the most widely used rail profile, characterized by a flat base with angled sides forming an inverted "V" shape (Figure 2.3.b). The characteristics of the profile grant great stability, ease of installation, manufacturing, and compatibility with a wide range of rolling stock. This profile offers cost-effectiveness, interchangeability, and seamless integration with rail fastening systems, ensuring efficient and reliable railway operations.

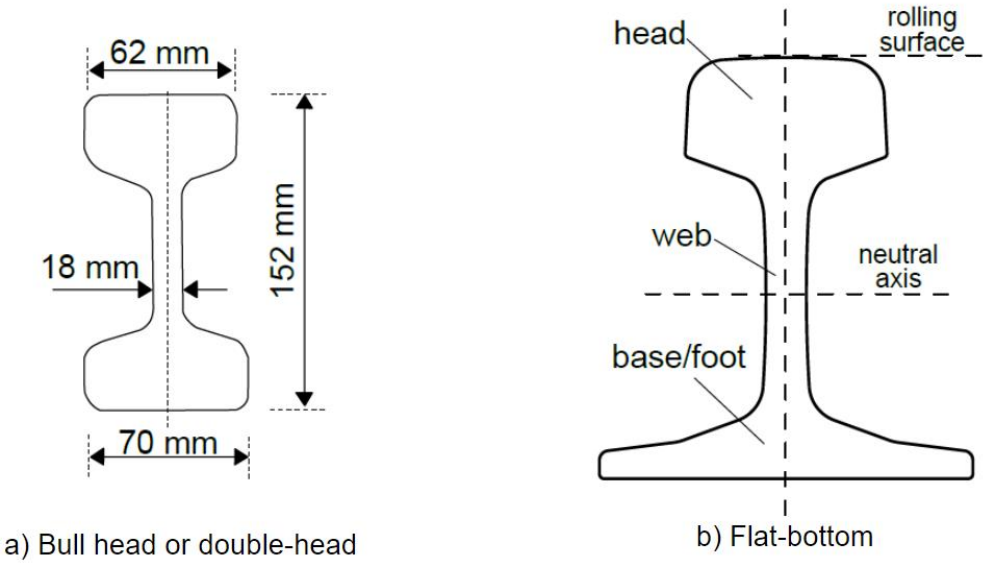

Figure 2.3 - Typical rail geometries. Adapted from [10].

To establish a standard for rail profiles used in different countries, specific documents outlining the specifications for geometry, manufacturing, and maintenance were developed. In the United States, the American Railway Engineering and Maintenance-of-Way Association is responsible for this task. In Europe, the European Standard EN 13674 is utilized. Generally, rail profiles are named based on their linear mass. For instance, profile 132RE represents a rail weighing 132 pounds per yard, while profile 136RE corresponds to a rail weighing 136 pounds per yard.

Table 2.1 - Rail profiles parameters [11]

Country	Rail section	A [m^2]	I_y [m^4]	I_z [m^4]
France	U33	$5906\ 10^{-6}$	$1588\ 10^{-8}$	$338\ 10^{-8}$
	U35-U50	$6450\ 10^{-6}$	$2019\ 10^{-8}$	$405\ 10^{-8}$
Germany	S49	$6296\ 10^{-6}$	$1819\ 10^{-8}$	$320\ 10^{-8}$
	S54	$6948\ 10^{-6}$	$2073\ 10^{-8}$	$359\ 10^{-8}$
Great Britain	BS110A	$6950\ 10^{-6}$	$2345\ 10^{-8}$	$417\ 10^{-8}$
	BS113A	$7150\ 10^{-6}$	$3349\ 10^{-8}$	$418\ 10^{-8}$
Ireland	85 lb/yard	$5370\ 10^{-6}$	$1154\ 10^{-8}$	$290\ 10^{-8}$
	92 lb/yard	$5943\ 10^{-6}$	$1586\ 10^{-8}$	$293\ 10^{-8}$
Japan	50N	$6405\ 10^{-6}$	$1960\ 10^{-8}$	$322\ 10^{-8}$
	50T	$6783\ 10^{-6}$	$2279\ 10^{-8}$	$380\ 10^{-8}$
	60	$7750\ 10^{-6}$	$3090\ 10^{-8}$	$512\ 10^{-8}$
Netherlands	NP46	$5930\ 10^{-6}$	$1605\ 10^{-8}$	$308\ 10^{-8}$
Switzerland	SBB1	$5880\ 10^{-6}$	$1631\ 10^{-8}$	$298\ 10^{-8}$
	UIC54E	$6860\ 10^{-6}$	$2308\ 10^{-8}$	$342\ 10^{-8}$
UIC	UIC54	$6934\ 10^{-6}$	$2346\ 10^{-8}$	$418\ 10^{-8}$
	UIC60	$7686\ 10^{-6}$	$3055\ 10^{-8}$	$513\ 10^{-8}$
USA	AREA132	$8355\ 10^{-6}$	$3671\ 10^{-8}$	$607\ 10^{-8}$
	AREA136	$8612\ 10^{-6}$	$3950\ 10^{-8}$	$612\ 10^{-8}$

Also, from Table 2.1, it can be observed that the inertia in the vertical direction is approximately five to six times higher than in the lateral direction. This significant difference in inertia helps to understand why, in the majority of cases, bending or deformation takes place primarily in the horizontal plane.

2.1.2. Sleepers

Railway sleepers, also known as railroad ties, are of most importance in the construction and operation of railway tracks. As elements of the track structure, individual cross ties receive loads from the rails or fastenings and transmit them to the ballast and subgrade [12]. They provide support and stability by creating a stable and level base for the tracks, distributing the weight of trains evenly, and preventing track sinking and misalignment. They are fundamental to

maintaining the correct track gauge. Additionally, sleepers absorb vibrations generated by trains, resulting in a comfortable ride for passengers and less wear on track components. Sleepers are also cost-effective, allowing for efficient maintenance and repair operations.

Railway sleepers are typically constructed from wood, concrete, or steel. These materials vary in terms of cost, operational characteristics, maintenance requirements, and the level of lateral resistance they offer to the ballast. Recent studies have focused on investigating the impact of altering the sleeper material on its ability to provide resistance [13], [14]. The standard geometry of the sleepers varies within different countries, but the main types used today are the monoblocs and bi-blocks, see Figure 2.4. To specify the exact geometry, it's necessary to take into account the rail gauge, fastenings, ballast and sub-ballast quality, manufacturing, installation, maintenance, durability, traffic loads, and environmental factors [12].

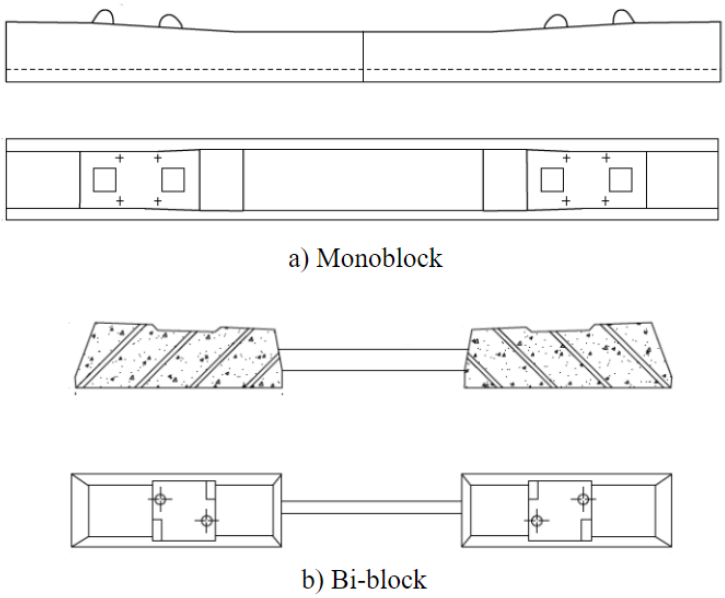

Figure 2.4 - Typical sleeper geometry type. Adapted from [15].

2.1.3. Ballast

Railway ballast, typically composed of crushed stone typically ranging from 28 mm to 50 mm in size [1], forms the foundation on which sleepers rest in the railway system. It fulfils a multitude of crucial functions within the railway infrastructure. Primarily, it helps in the dispersion of stresses transmitted from wagons through the sleepers, ensuring a uniform distribution of the load. Furthermore, acting as a cushioning material, it can mitigate train vibrations. Additionally, ballast exhibits resistance against track displacement in both transverse and longitudinal directions, thereby upholding track stability and helping to prevent track buckling. Track ballast is also an efficient rainwater drainage, thus preventing the accumulation of water and associated complications. In essence, railway ballast assumes a very important role in stress distribution, vibration attenuation, track stability, drainage, and expedient track maintenance within the railway system [15].

In constructed and operational railway tracks, the ballast layer can be divided into four zones, see Figure 2.5. Crib ballast is the ballast area located between the sleepers. The shoulder ballast extends from the end of the sleeper to the top of the sub-ballast and has a sloping configuration. The top ballast corresponds to the upper part of the ballast structure and typically is subjected to tamping. Finally, the bottom ballast constitutes the lower portion of the structure that provides support to the overall system. The specific characteristics and performance of each zone are influenced by factors such as the quality of the sub-ballast material, loading conditions, as well as the presence of water and drainage properties within the structure [16].

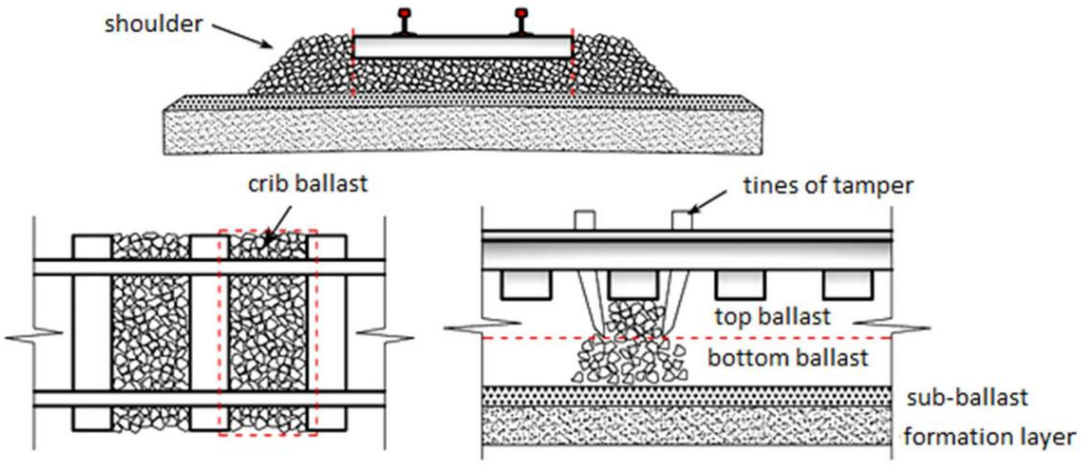

Figure 2.5 - Ballast subdivisions [16]

2.1.4. Fasteners

Fasteners are the mechanisms that connect the sleeper to the rails. They provide torsional resistance between them. According to Profillidis [15], these are the main characteristic that the fasteners should provide to the rail system:

- Maintaining the track gauge as closely as possible to its nominal value;
- Ensuring a consistent rail inclination on the sleeper;
- Transferring loads effectively from the rail to the sleeper;
- Attenuating and dampening vibrations caused by train traffic;
- Allowing for easy installation and maintenance;
- Providing electrical insulation properties;
- Exhibiting resilience and adequate deflection.
- Preventing abrasion between components and over-stressing.
- Offering resistance to corrosion.

Fasteners used in railway tracks can be categorized into two main groups: rigid and elastic fasteners. Rigid fasteners are specifically designed for wood or steel sleepers and are typically secured using nails or bolts, see Figure 2.6. In some cases, rigid plates may also be utilized beneath the rails. It's important to note that rigid fasteners are not suitable for other types of sleepers.

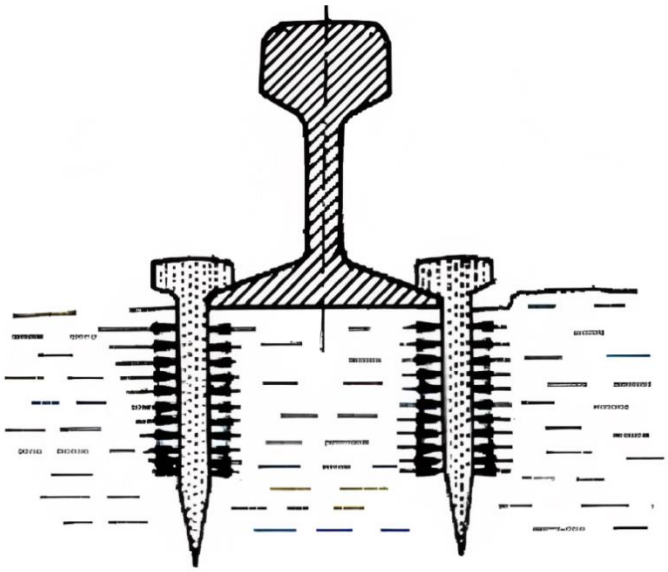

Figure 2.6 - Rigid fastener [15]

Elastic fasteners offer greater versatility as they can be utilized on various types of sleepers, including concrete, wood, and steel. They also provide effective electrical insulation between the rail and the sleeper. Within the category of elastic fasteners, there are two subtypes: screw-type fasteners and spring-type fasteners. Screw-type fasteners involve a screw that is attached to the sleeper, which applies pressure on a spring steel element, often a steel plate (Figure 2.7a). On the other hand, spring type elastic fasteners rely on a spring component that generates clamping force to secure the rail and sleeper together (Figure 2.7b).

a) Screw Type b) Spring Type

Figure 2.7 - Elastic fasteners [15]

2.2. Railway Buckling

Buckling denotes a mechanical instability inherent to structural systems exposed to compressive loads. This phenomenon manifests when slender structural elements, such as columns or beams, experience compression, resulting in unanticipated lateral deflection or buckling rather than sustaining their linear configuration while bearing the load. Typically, buckling occurs when the compressive load exceeds a critical threshold. It is influenced by various factors such as boundary conditions, level of imperfections, and the applied load. In the case of railways, thermal and mechanical loads can lead to buckling under certain conditions. Continuously welded rails (CWR) are more susceptible to this phenomenon compared to jointed rails because they restrict longitudinal movement and convert thermal deformation into internal stresses. Once the buckling limit is exceeded, the rail's stable shape is lost, and it undergoes sudden and significant lateral movement, eventually settling into a new deformed shape, as it’s shown in Figure 2.8.

Figure 2.8 - Buckled railway

Depending on the prevailing conditions, buckling can manifest in two distinct forms: explosive buckling or progressive buckling. Explosive buckling is characterized by a catastrophic failure, wherein stored energy is swiftly and almost instantaneously released. Conversely, progressive buckling typically arises from a gradual dissipation of compressive energy accumulated within the structural element.

In the context of rail buckling, the occurrence of explosive buckling is typically contingent upon a higher resistance to buckling displacement [7]. This resistance primarily emanates from the lateral and longitudinal ballast resistance. When robust ballast resistance is present, it is more probable to observe explosive buckling. Conversely, in scenarios where ballast resistance is weaker, progressive buckling tends to be more prevalent. Figure 2.9 presents the typical curves for explosive and progressive buckling.

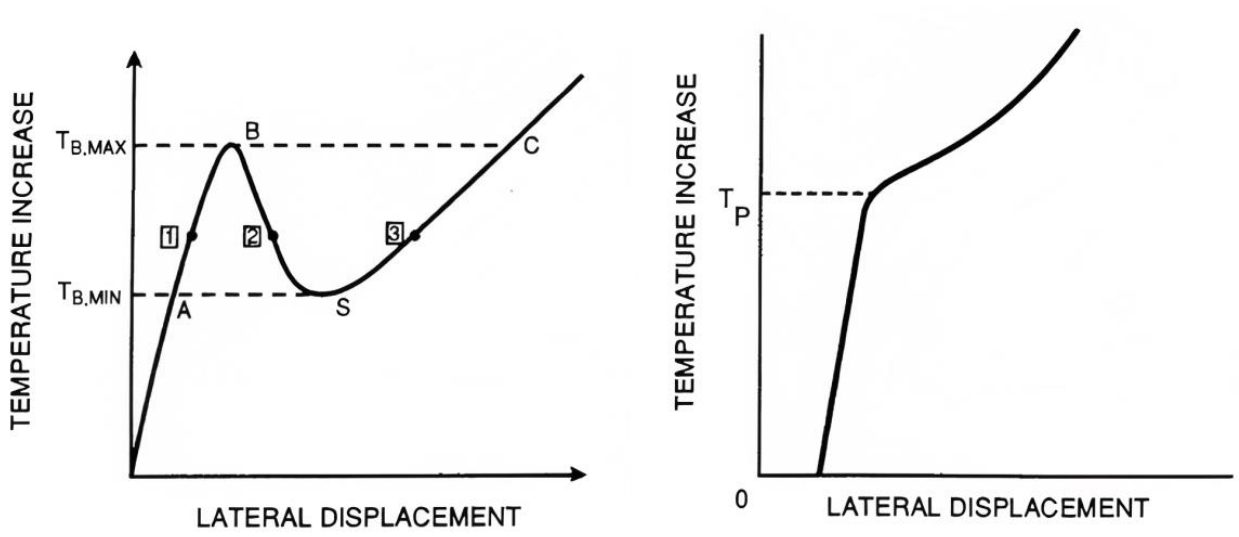

(a) Explosive Buckling Response (b) Progressive Buckling Response

Figure 2.9 - Typical track buckling response curves [17]

2.2.1. Experimental Tests

In 1982 [18] experimental tests were conducted about the buckling of CWR railways for the United States Federal Railway Administration (FRA). The objective of the work was to validate the analytical studies made previously about CWR track buckling, safety concepts, and the safe temperatures of the railway so that buckling does not occur. The work consisted of static experimental tests of thermal buckling on an existing rail line in the city of The Plains, state of Virginia. Curved and straight railway lines were tested with an initial imperfection in the middle of the 200m total rail length.

The experimental procedure started by obtaining the stress-free temperature of the rails. Both ends of the track were cut, the rail anchors were removed, and the rail de-stressing occur. With this, the authors obtained a stress-free temperature of approximately 22°C for both straight and curved

tracks. This temperature will be used as a reference for the variation of temperatures when measuring the track displacement. With the help of a bulldozer, the sinusoidal wave shape imperfections were introduced in the straight and curved tracks. After the track settle down, the measurements were made and resulted in imperfections with 4 millimetres of amplitude perpendicular to the rail and had approximately a longitudinal length of 11 meters, as shown in Figure 2.10. Considering that the imperfections have an axis of symmetry in the middle of their length, the figure below represents only half of the imperfections.

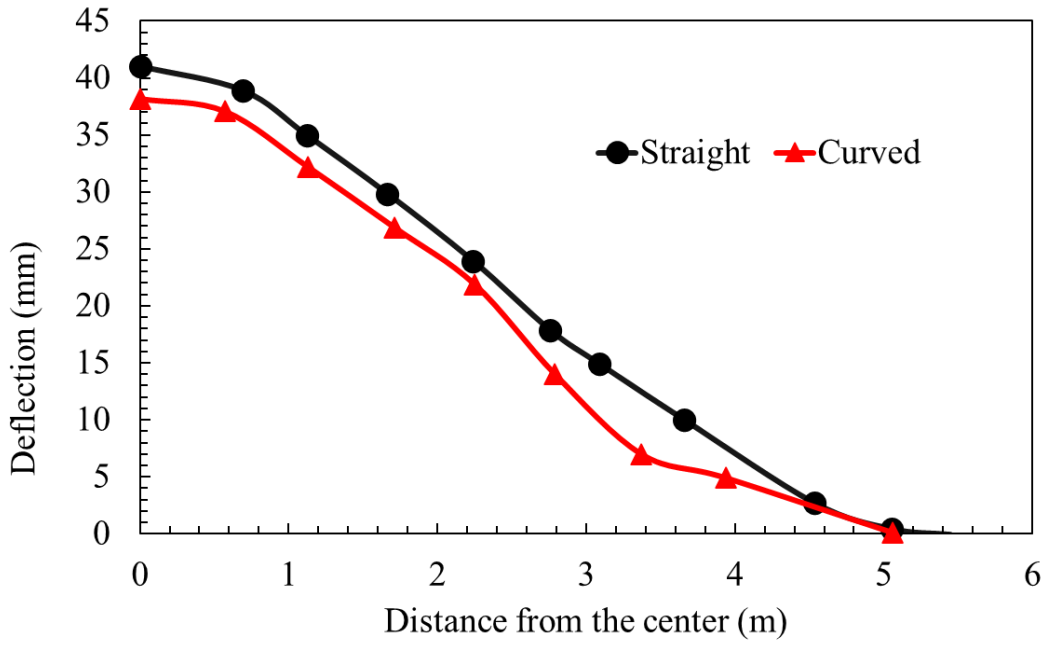

Figure 2.10 - Initial misalignment from experimental test. Adapted from [17]

For the rail temperature variation, electric resistance heating was applied using 2 locomotives, one on each rail end. In addition to providing rail heating, locomotives also served to assist in anchoring the ends of the test. However, one drawback of the experiment is that this heating method does not ensure a consistent temperature across the entire rail. With the increased rail temperatures, the

authors could collect data about the rail temperatures and displacement and compare it with the theoretical predictions that were previously made.

2.2.2. Numerical Models

Numerical models are often used to simulate and evaluate the behaviour of railroad tracks. To predict the likelihood of rail buckling, these models make use of mathematical algorithms and finite element techniques. These numerical models can determine the risk of rail buckling and assist in the design of preventive measures, such as rail fasteners and heat management strategies, ensuring the safe and effective operation of rail networks.

In their 2003 study, Lim et al. [7] developed a three-dimensional CWR track model specifically designed to analyze the buckling behaviour of CWR tracks under temperature loads. The model utilized a specialized finite element method program and included four elements: a mono-symmetric thin-walled open section beam element representing the rail, a solid beam-on-elastic-foundation element simulating the tie, elastic spring elements for the pad-fastener system, and spring elements accounting for lateral or longitudinal ballast resistances, as illustrated on Figure 2.11.

In their study, a 200m rail was modelled, with a rail gauge of 1435mm and a rail profile of 132RE. Three models were tested, the first model had the rail ends fixed and the lateral, longitudinal, and vertical displacements were constrained. In the second and third models, the rail ends were not fixed, instead, the authors proposed a longitudinal constraint on the end of the rails with a certain elastic stiffness behaviour, to better reproduce the experimental tests [18].

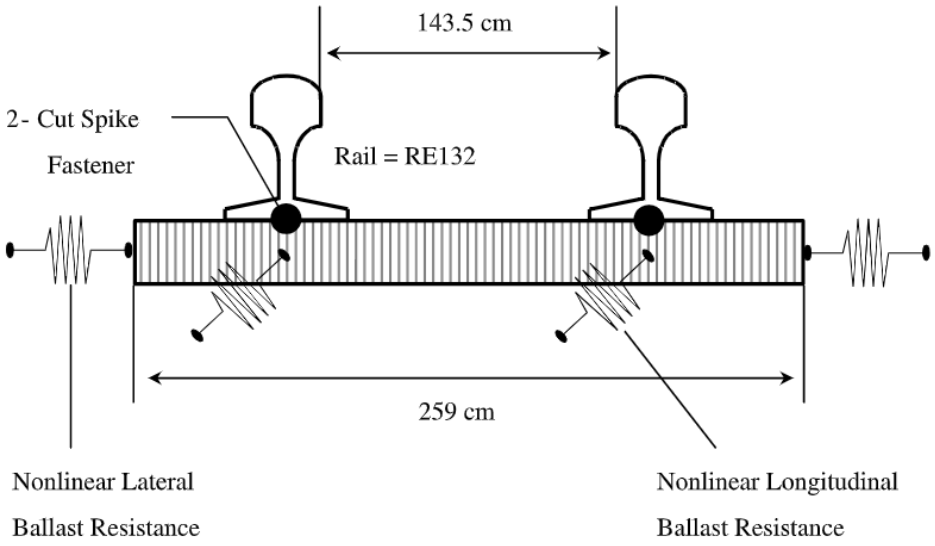

Figure 2.11 - Railway model representation. Adapted from [7]

Comparative analyses were performed to validate the model against previous research that utilized 2-D models as well as the previous experimental work made by Kish et al. [18]. The findings emphasized that track buckling is a three-dimensional phenomenon, suggesting that conventional 2-D rail-tie models and beam models tended to overestimate the stability of CWR tracks.

Pucillo in 2016 [19], studied the rail buckling phenomenon using the numerical model in ABAQUS. Both rail and sleeper were considered as beam elements in the simulations and the connection between them was simulated as a torsional spring. For the ballast-sleeper interaction, an elastoplastic behaviour was adopted on the lateral spring used to simulate the ballast resistance. For the longitudinal resistance of the sleeper, an elastic spring was considered. The misalignment of the track was introduced in the middle of the tested length and had a lateral amplitude of 5 millimetres and 20 millimetres. The simulations were made considering lengths of 24 48 120 and 240 meters with both extremities of the rails fixed.

Also, Pucillo [20] conducted a parametric study in 2019 about railway buckling. For modelling the experiment, he utilized the finite element model in ABAQUS, utilized by him in his previous work and validated with other analytical studies. however, this model has a difference from the previous ones, it considers the bending stiffness of the whole track considering the horizontal plane.

Both the ties and the rails were considered beam elements in the model. The fastener's representation as well as lateral and longitudinal ballast resistances were inserted in the model as connectors. For the lateral and longitudinal resistances, Pucillo considered the resistances between the ballast-sleeper interaction as nonlinear springs, with an elastoplastic behaviour.

To prevent the model from suffering the snap-trough phenomenon that happens between the buckling temperature $\Delta Tmax$ and the safe temperature $\Delta Tmin$, Pucillo utilized the arc length method, which is described in the ABAQUS software as the Modified Riks Algorithm. The phenomenon represented in Figure 2.12 consists of the incorrect representation of the buckling curve, where from point A, the equilibrium point moves directly to point B and consequently to point C.

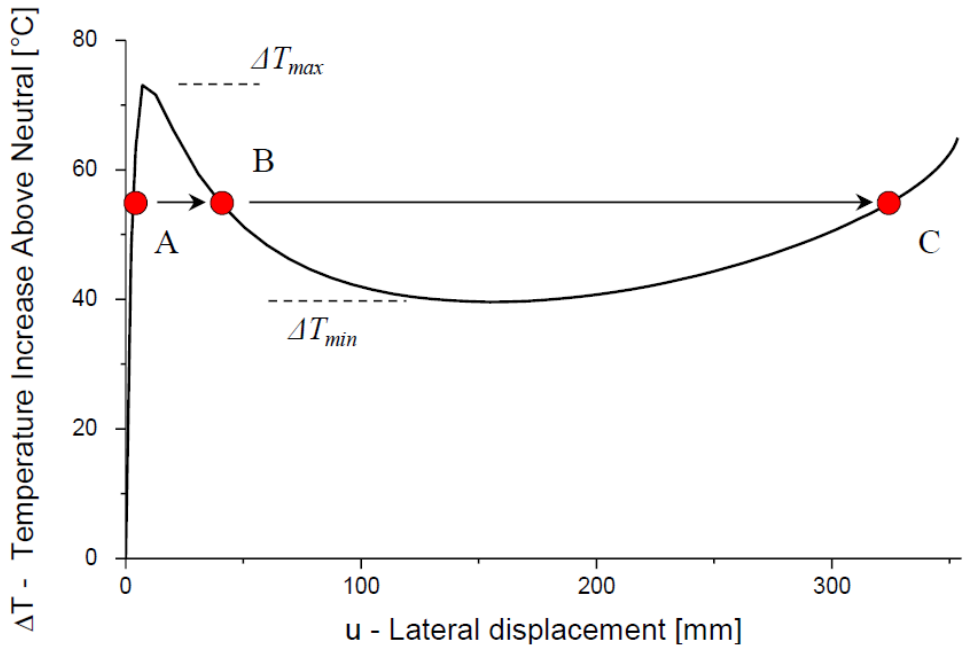

Figure 2.12 - Explosive buckling curve [20]

The validation that the authors made was a comparison with another finite element model of thermal railway buckling made by Lim et al. [7]. The railway buckling phenomenon was simulated in ABAQUS, with an initial imperfection in the middle of the track and continuously increasing temperature. Results showed good agreement with the reference literature.

Subsequently, parametric studies were conducted on the dynamic buckling of railways to evaluate the influence of mainly two parameters, the truck centre spacing and the bogies axle spacing. The conclusion showed that increasing the truck centre spacing and decreasing the initial misalignment will increase the difference between *ΔTmax* and *ΔTmin* as shown in Figure 2.13. This difference implies that explosive buckling will happen as opposed to progressive buckling, which occurs when *ΔTmax* is very close *ΔTmin*.

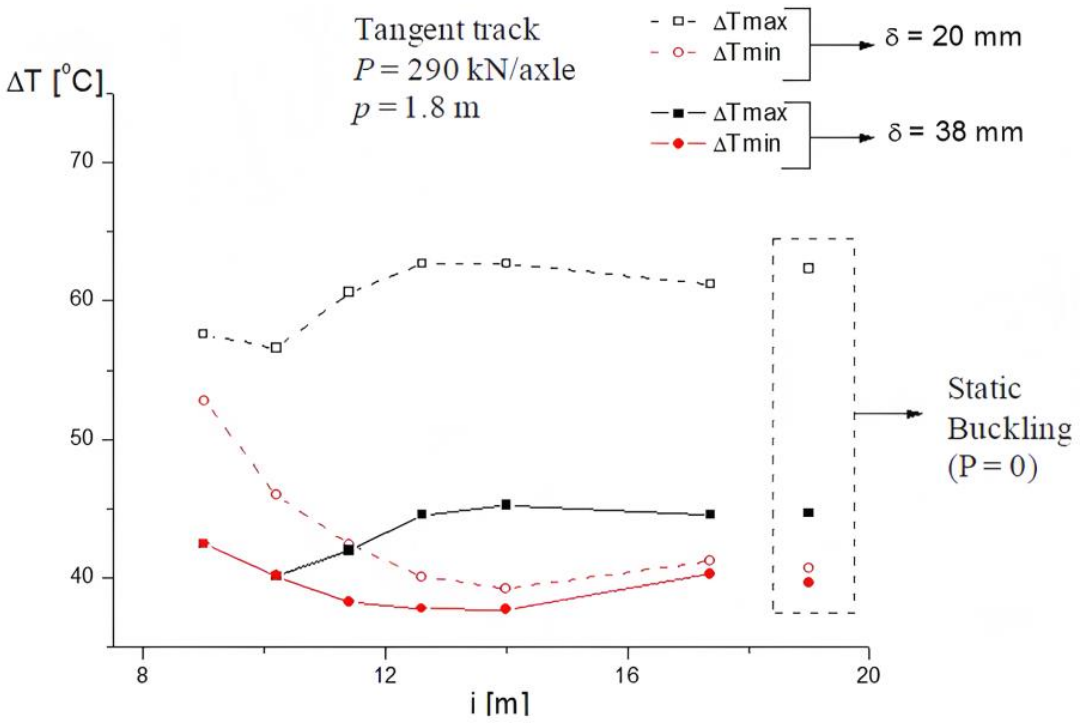

Figure 2.13 - Truck centre spacing influence on track buckling. Adapted from [20]

In 2021 Miri et al. [21] compared static and dynamic track buckling using a multi-body train-track dynamic model and a 3D finite element track model. The study examines various scenarios, including static thermal analysis, dynamic analysis of a wagon with steady motion at a constant speed, dynamic analysis of a wagon with defect-free wheels during braking, and dynamic analysis of a wagon with out-of-round defect wheels during braking. For representing the forces exerted by the bogie wheels on the rail, the authors used the quasi-static load idealization, based on the assumptions made by previous work [22]. The authors utilized a 3D finite element model of the track developed in ABAQUS to simulate the railway elements. The model was carefully constructed to account for the non-linear interaction between the sleepers and ballast material in both lateral and longitudinal directions.

To analyze the track's susceptibility to buckling, the authors applied the wheel-rail quasi-static loads to the rails. Subsequently, they employed the modified RIKS method available in Abaqus to gradually increase the rail temperature. The RIKS method facilitated the incremental application of a portion of the total load to the model. An equilibrium iteration check was performed at each increment to ensure stability before progressing to the next load increment. This iterative process enabled the determination of buckling behaviour and the identification of safe temperature ranges for the track. The results indicate that train loads have a significant impact on both the buckling temperature and the safe temperature.

In 2021, Frigeri et al. [10] conducted a parametric study on static rail buckling. They used a numerical model developed in Ansys, based on the Newton Raphson method, to simulate the buckling behaviour. The rail and sleepers were represented using BEAM188 elements, the meshed model is shown in Figure 2.14. To account for the torsional stiffness of the fasteners and the lateral and longitudinal resistance of the ballast, COMBIN39 elements were employed. The resistance applied by the ballast as well as the fastener’s torsional stiffness were derived from previous research [17] [23], linearized, and assumed to exhibit multilinear behaviour. The rail elements were gradually heated from 20 °C to 200 °C over a duration of 200 seconds.

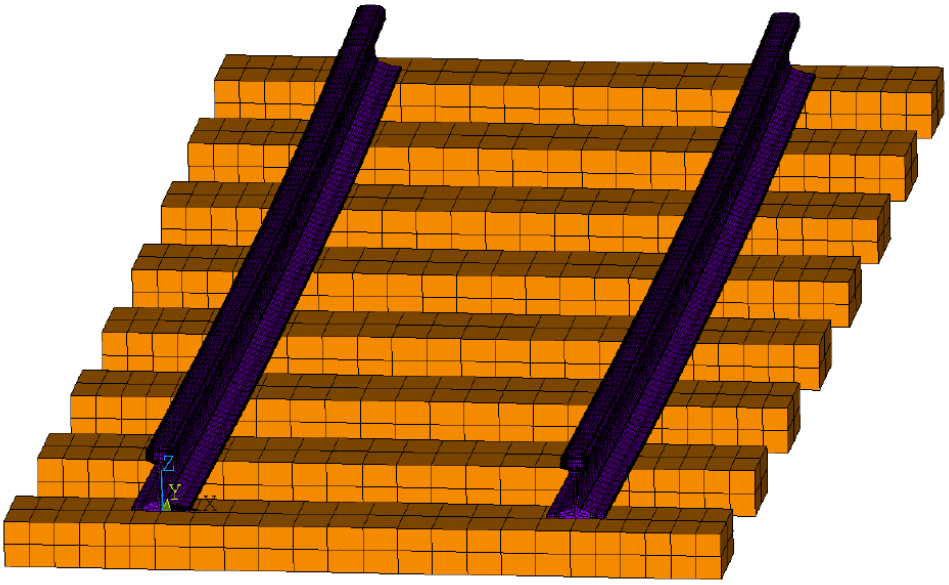

Figure 2.14 - BEAM188 elements [10]

The model had an initial imperfection on the longitudinal central node of both rails (Y-axis direction), which was later varied on amplitude for the parametric analysis A total of 144 simulations were made by the authors. The analyzed parameters follow in Table 2.2.

Table 2.2 - Parameters analyzed. Adapted from [10].

Rail Profile	**Gauge (mm)**	**Imperfection L_0**	**E Sleeper (GPa)**	**Ballast Resistance**	**Fastener (kNmrad^{-1})**
UIC54	1000	200	3.4	Weak	43
UIC60	1435	500	16	Strong	135
	1664	1000			

The authors did not consider that wood and concrete materials have different tie-ballast strengths, longitudinally and laterally. The stiffness of the fasteners also varies with different sleeper materials. In addition, the authors used a rail length of 4.2 meters, which was demonstrated by Lim

et [24] that this length can produce inaccurate results. Without the use of other artifices on the numerical model, like infinite boundary elements, simulations with shorter rail lengths do not converge to the results obtained with larger rail lengths, presenting incorrect values of safe rail temperature.

2.2.3. Analytical Models

In 1978, Kerr [25] conducted a study to determine the permissible temperature range for safe temperature increases, focusing on explaining the occurrence of track buckling using the minimum potential energy buckling theory. The study employed non-linear mathematical formulations, but exact solutions were obtained through precise calculations, presenting four buckled configurations. Additionally, a simplified model of the lateral resistance of the ballast into the sleeper is taken into consideration, based on a beam model that did not consider the torsional stiffness as an individual element. Since the author considered rail tracks that use cut spikes fasteners, Kerr considered this parameter negligible and did not include it individually in the analysis.

The analytical model was used in 2015 by Navarro et al. [26] to simulate the railway buckling phenomenon for both unloaded and loaded tracks. Their study substituted the rail sleeper structure with a respective beam model considering the same cross-section and inertia. The authors did not consider explicitly the influence of the fastener's rigidity. Instead of that, they increased the lateral resistance of the ballast to compensate for it. The model is designed with initial misalignments in two shapes: a half-wave and a full-wave sinusoidal curve. A compressive load P will be applied in both of the misalignment ends. Rigidity presented by the sleeper about the ballast was

considered in the compressed end of the sleeper as passive earth pressure and on lateral and under sides as the friction between the ballast–sleeper surfaces.

For the sleeper resistance, the vertical load applied by the train load or the track weight itself and the surface friction coefficient were the most relevant parameters that the authors considered in their work. For comparison reasons, two different sleeper materials were chosen for the test, wood, and concrete, which differ mainly in their surface friction coefficients. The ballast maintenance condition was considered in this work, varying mostly the lateral resistance of the track. In addition, the concrete sleeper shape is variated in single-block concrete sleepers and twin-block concrete sleepers.

The model resolution was made using the energy equilibrium method, utilizing the following equation 2.1 is the total potential energy of the comprised track and *Wp* is the work of external forces, in this case, the force *P*.

$$V(y0, L, F) = Ubending + Uballast - WP \quad (2.1)$$

Parametric studies were conducted varying the parameters presented in Table 2.3. Furthermore, unloaded rail and loaded rail cases were both analyzed. After all possible parameter combinations are concluded, statistical treatment has been applied for both loaded and unloaded cases.

Table 2.3 - Parameters analyzed. Adapted from [26].

Parameter	Analyzed levels		
Sleeper Type	Wooden Monoblock	Concrete Monoblock	Concrete Bi-Block
Track Maintenance Conditions	Consolidated	Tamped	Stabilized
Rail type	UIC54	UIC60	
Amplitude of Misalignment	1 cm	5 cm	2.5 cm
Form of Misalignment	Half Wave	Full Wave	
Sleeper Ballast Coverage	Full	Full-5 cm	

To analyze the parameter's influence on the buckling load, the global effect of the individual parameters was calculated and it is presented in Table 2.4. Knowing the global importance of the parameters, those responsible for the projects and maintenance of railways know which points need more attention and care, to avoid buckling of the railway.

Table 2.4 - Influence of Buckling Parameters. Adapted from [26].

	Unloaded Track	Loaded Track
Sleeper Type	16.9%	2.0%
Rail Type	6.8%	3.4%
Amplitude of Misalignment	52.6%	61.2%
Form of Misalignment	5.3%	8.5%
Maintenance of Ballast	16.2%	1.9%
Sleeper Ballast Coverage	2.4%	0.0%

Results obtained by the authors showed that the loaded tracks have a 200% higher buckling load than the unloaded tracks. Furthermore, the study showed that the parameters that most influence track buckling are the sleeper type, track maintenance, and misalignment amplitude.

In 1993, Van [23] conducted a sensitivity analysis aimed at determining the key parameters influencing the stability of track models. The author modelled a curved track with a total length of 47.5 m and a radius of 400 m. An initial imperfection was inserted at the middle of the track on both rails varying from 0.008 to 0.05 m in amplitude. Parameters such as the longitudinal and lateral resistances of the ballast were set with a multilinear behavior, based on previous studies. Van also considered in his study the influence of force applied by a hopper car, on each of the four wheels with a vertical load of 293 kN each.

The study revealed that curvature, horizontal ballast strength, and misalignment were the most influential factors contributing to rail buckling. Additionally, the research indicated that highly rigid fasteners offered substantial enhancements to track stability, while the stiffness of fasteners, longitudinal and lateral ballast played a relatively minor role in comparison.

2.3. Buckling Parameters

Studying rail buckling parameters involves exploring different factors that affect how susceptible rails are to buckling under certain conditions. The most crucial parameters englobe characteristics like rail material properties, rail geometry, track configuration, fastener stiffness, and ballast resistance. Each of these factors influences how likely rail tracks are to buckle, so understanding their impact is important for designing and maintaining safe and strong rail infrastructure. It's

crucial to have knowledge of these factors and how each one affects rail buckling to ensure the safety and durability of rail networks, avoiding the necessity to stop rail traffic for safety-related issues.

2.3.1. Sleeper-Ballast Resistance

One of the many importance of the ballast on railways is to provide a certain resistance to the sleepers, acting against the forces generated by the train passage and the thermal strains of the rail. This resistance is crucial for maintaining track alignment, preventing excessive deformation or settlement, and ensuring the safe and efficient operation of trains. Numerical models, to simplify the modulation of the real-world conditions, separate the ballast resistance into lateral resistance and longitudinal resistance.

The most adopted method to evaluate the lateral resistance of the ballast is the single tie push test (STPT). This method consists of pushing or pulling an individual sleeper, measuring the force applied, and the respective lateral displacement. Data prevenient from previous research [23] show the lateral resistance for both compacted and tamped ballast conditions for the wood sleeper case, see Figure 2.15. The consolidated ballast condition shows a peak resistance value that isn't present in the looser ballast case. As the displacement increases, the ballast compaction is gradually reduced, until finally the resistance of the compacted ballast equals the uncompacted case.

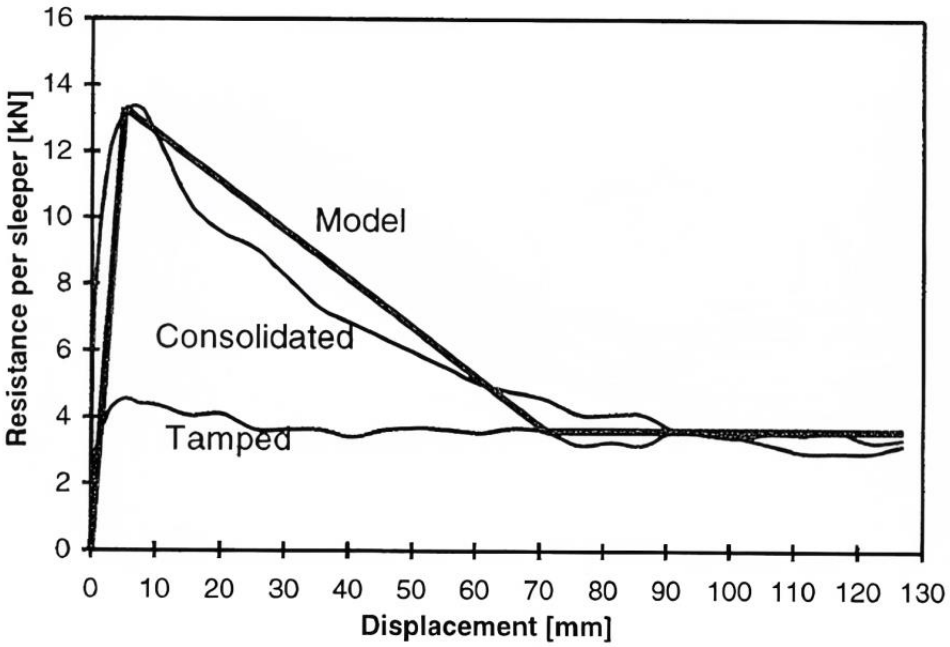

Figure 2.15 - Typical lateral resistance response [23]

It is important to note that the lateral resistance undergoes variation as rail wagons traverse the track. This variation is attributed to the loads exerted on the rails by the wheels of the bogies, as illustrated in Figure 2.16. As a result, the normal forces applied by the sleepers onto the ballast are heightened, leading to an increase in the frictional force between them. Consequently, the lateral and longitudinal resistance between the sleeper and ballast is also increased.

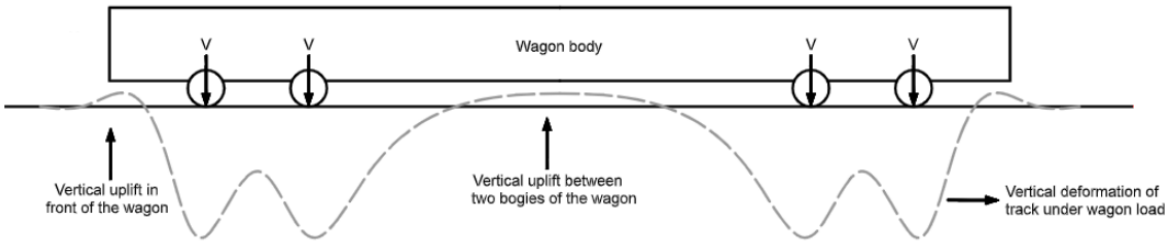

Figure 2.16 - Vertical uplift caused by rail wagons. Adapted from [21].

On the other hand, the track portion that is located between de rail cart bogies suffers a vertical uplift. As a consequence, the lateral resistance on this part of the track gets weaker. The variation in the lateral resistances inflected by the passing of rail carts is shown in Figure 2.17.

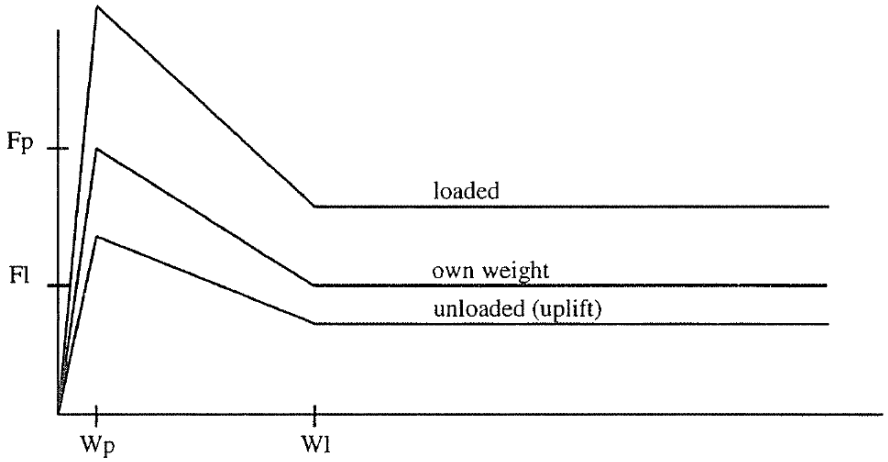

Figure 2.17 - Influence of vertical force of wagons on the lateral resistance [23]

In 2013, Zakeri et al. [13] experimented with different types of sleepers to evaluate the difference in lateral resistance. The major parameter analyzed was the sleeper's material, specifically the wood, concrete, and steel sleepers. Wooden sleepers presented the lowest lateral resistance. Steel ties presented an increase of 7.3% in total lateral resistance compared to the wood case. Concrete sleepers showed the highest lateral resistance, increasing by 27.8% compared the wood sleeper sleepers.

In 2023, Dersch et al. [14] studied the influence of a series of parameters regarding the longitudinal resistance of the ballast. In their work, a series of track panel push tests (TPPT) was conducted, consisting of two hydraulic actuators placed on the rail ends that pushed both rails in the longitudinal direction. The track configuration included 10 sleepers, rails, fasteners, and ballast.

For the parametric analysis, sleeper materials, fasteners, and ballast conditions were modified to evaluate each parameter's influence on the general longitudinal resistance. The results are presented in Figure 2.18 and the parameters adopted on each track configuration are shown in Table 2.5.

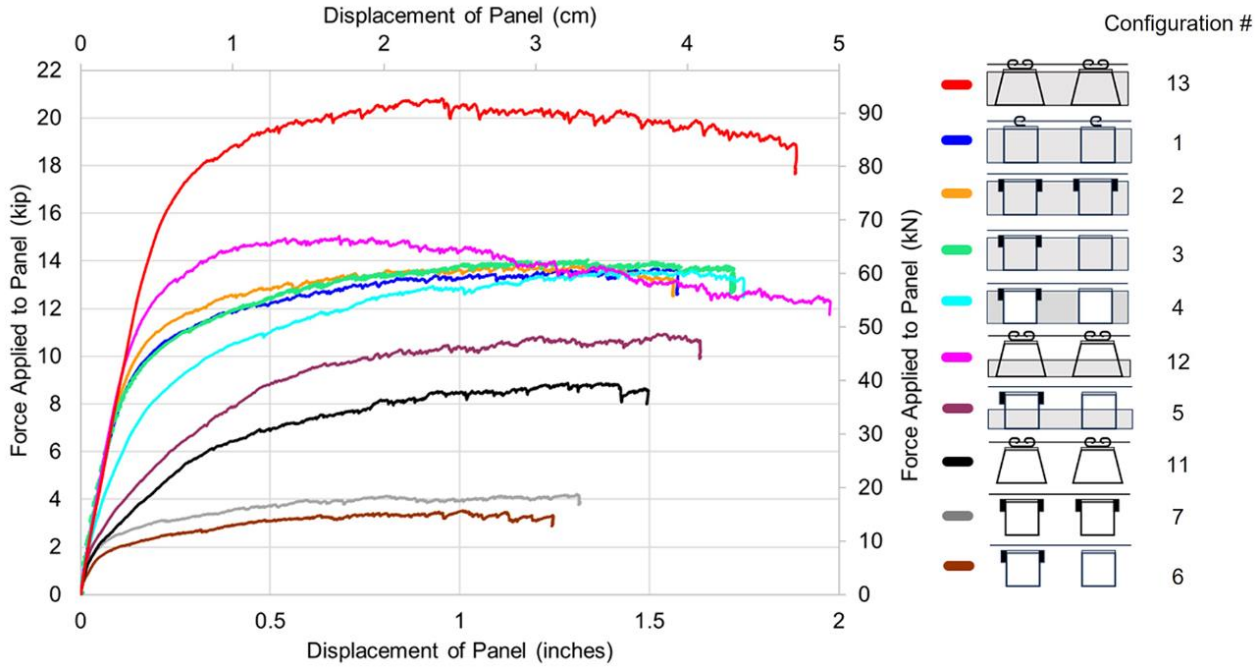

Figure 2.18 - Longitudinal resistance for different track configurations [14]

Table 2.5 - Parameters for longitudinal resistance tests. Adapted from [14].

Configuration	Sleeper Type	Crib Ballast Height	Fastener	Shoulder width	Legend
1	Timber	Full	Spikes and elastic fasteners	12 in.	
2	Timber	Full	Spikes and ETA	12 in.	
3	Timber	Full	Spikes and EOTA	12 in.	
4	Timber	Full	Spikes and EOTA	0 in.	
5	Timber	Half	Spikes and EOTA	12 in.	
6	Timber	Empty	Spikes and EOTA	12 in.	
7	Timber	Empty	Spikes and ETA	12 in.	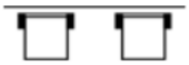
8	Timber	‘‘Frozen’’	Spikes and ETA	12 in.	na
9	Timber	‘‘Frozen’’	Spikes and EOTA	12 in.	na
10	Concrete	‘‘Frozen’’	Elastic Fasteners	12 in.	na
11	Concrete	Empty	Elastic Fasteners	12 in.	
12	Concrete	Half	Elastic Fasteners	12 in.	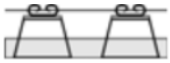
13	Concrete	Full	Elastic Fasteners	12 in.	

The authors tested variations of ballast conditions, including full, half, and no crib conditions. The ballast crib consists of the portion of the ballast located between the sleepers, see Figure 2.19.

Results obtained by the authors showed that the half crib ballast in comparison with the full crib ballast presents a 25% lower longitudinal resistance for concrete sleepers and an 18% lower longitudinal resistance for wood sleepers. Furthermore, the presence of the ballast shoulder did not affect considerably the longitudinal resistance, being the greatest effect on the loss of the ballast crib. As the displacement increases, the crib tends to escape from its original configuration, due to the lack of ballas shoulder, and consecutively decreasing longitudinal resistance.

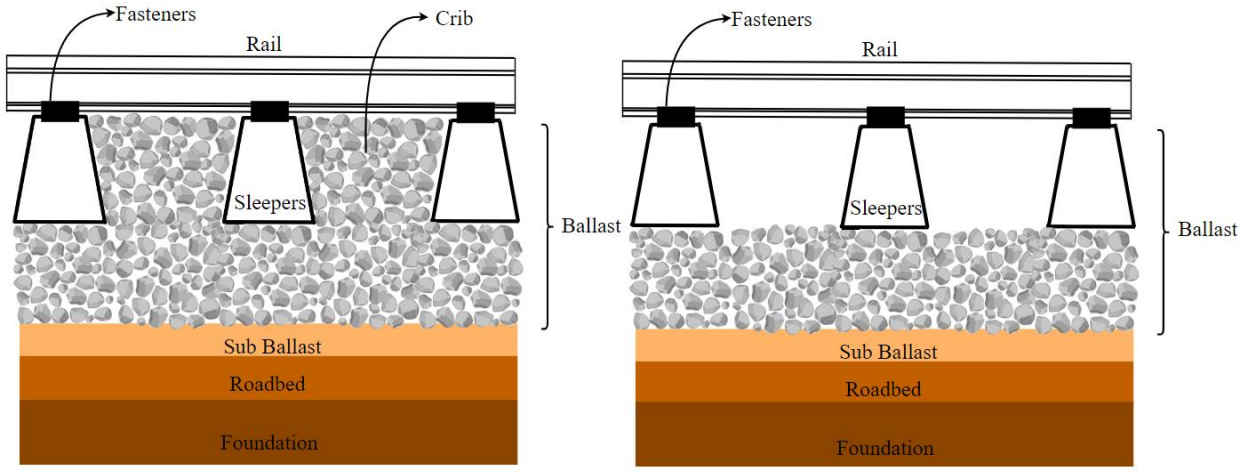

a) Typical ballast configuration b) No crib ballast configuration

Figure 2.19 - Different ballast configurations

2.3.2. Fasteners Torsional Stiffness

The fastener's torsional stiffness mainly depends on the fastener type and sleeper material that they are attached to. Generally, increasing the fastener stiffness results in a slightly higher buckling temperature [17]. To evaluate the rigidity provided by each fastener type, the sleeper is fixed and

a load is applied laterally on the rail. Then, the torque and the corresponding rotational angle are measured, generally presenting a linear behaviour as shown in Figure 2.20.

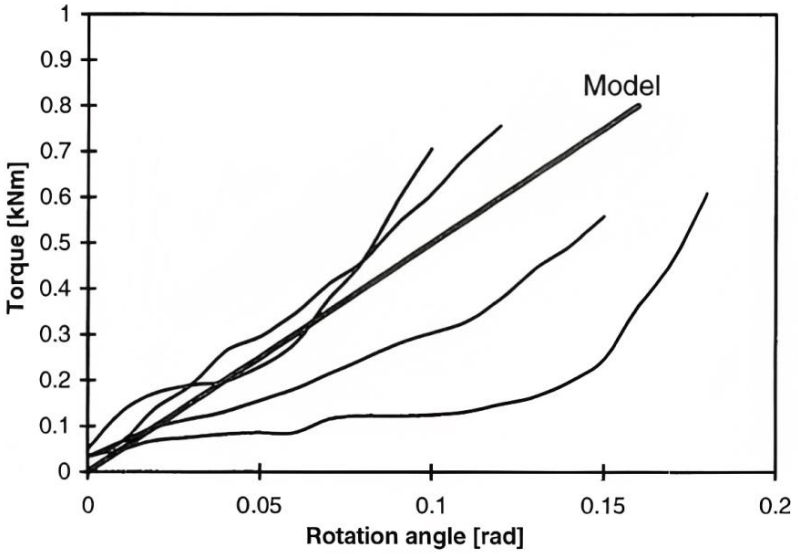

Figure 2.20 - Typical fastener rigidity response [23]

The experiment conducted by the Volpe National Transportation Systems Center (VNTSC) measured the torsional stiffness of different fastener systems and different sleeper materials [17], the results are presented in Table 2.6. From the results, it's clear that wood sleepers present higher torsion resistance values compared to concrete sleepers.

Table 2.6 - Torsional Stiffness Values [17]

	Fastener System	Average $\bar{\tau}_o$ (kips-in./rad)	σ	No. Tests
Wood ties	Pandrol	5026	1957	3
	8 spikes/plate	2165	589	6
	4 spikes/plate	1203	384	22
	2 spikes/plate	386	145	4
Concrete ties	Pandrol	281	159	7
	McKay Safeloks	343	83	10
σ = Standard Deviation				

2.3.3. Track Misalignments

For track buckling to take place, it is crucial to have an initial misalignment in the lateral plane [21], [27], [28]. As noted by the results of previous works [17] [29], rail misalignments are one of the most important parameters when analyzing the buckling temperature of railways. Generally, to reproduce the imperfection on rail models, a sinusoidal wave shape is introduced on the rail with a misalignment amplitude before rail buckling, represented as δ0, as shown in Figure 2.21. Misalignments can serve as an aggravator factor in railway failures. To ensure safety, maximum values for track misalignments have been established in consideration of this factor [30].

- δ_0 - refers to the misalignment deficiency that occurs after construction and operational maintenance, typically falling within the range of 1 to 4 mm.
- δ_m - represents the maximum permissible misalignment deficiency that is tolerable before maintenance becomes necessary, ranging from 4 to 8 mm.
- δ_c - denotes the critical misalignment deficiency that necessitates immediate maintenance due to the potential compromise of track safety.

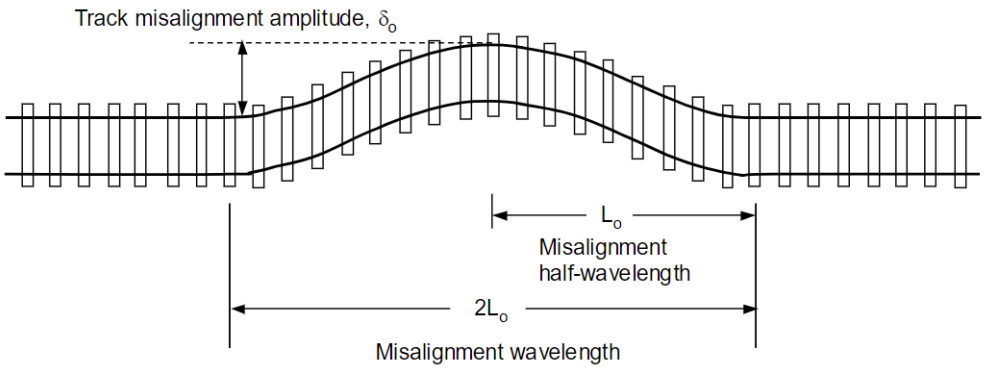

Figure 2.21 - Initial Misalignment [31]

2.3.4. Rail Geometrical Properties

The geometrical properties that are relevant to rail buckling are rail cross-sectional area, the cross-sectional moments of inertia for bending in both the vertical (I_{yy}) and horizontal (I_{zz}) planes, and the track self-weight [17]. Since the rail buckling phenomenon normally takes form in the lateral direction, the influence of the vertical section moment of inertia I_{yy} can be disregarded. These parameters influence the radius of gyration I and the slenderness ratio of the rail λ, as shown in equations 2.2 and 2.3. As the slenderness ratio of a column increases, it becomes more susceptible to buckling.

$$i = \sqrt{\frac{I_{zz}}{A}} \tag{2.2}$$

$$\lambda = \frac{l_e}{i} \tag{2.3}$$

For evaluating the influence of this parameter on buckling temperatures, previous works altered the rail profiles while maintaining other parameters as standard [17], see Figure 2.22. From the results, we can conclude. Although a smaller rail profile results in elevated buckling temperatures, it also leads to increased bending stresses induced by the wheel loads of rail carts.

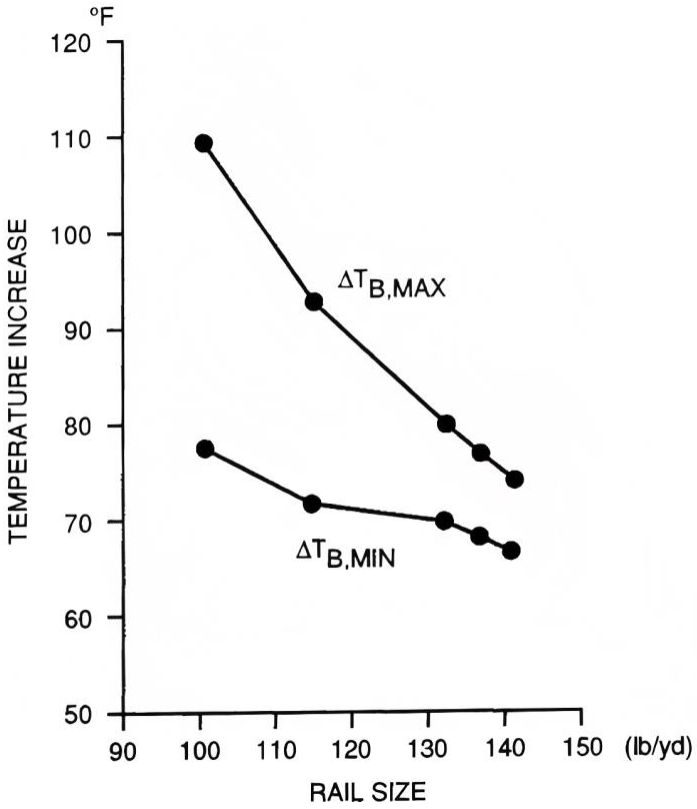

Figure 2.22 - Influence of rail size on buckling temperatures [17]

2.3.5. Track Curvature

The influence of track curvature has been previously studied by a series of authors [17]–[19], [22]. Rail curvature refers to the degree of curvature or bending of the railway tracks along their alignment. The presence of curvatures on the rails leads to lateral loads being applied to both rails. The differential loading between the inner and outer rail increases the chances of buckling. Since the railway curves are inevitable elements when constructing a railway, the countermeasure adopted by engineers to reduce the lateral forces was the implementation of superelevation on the outer rail, see Figure 2.23.

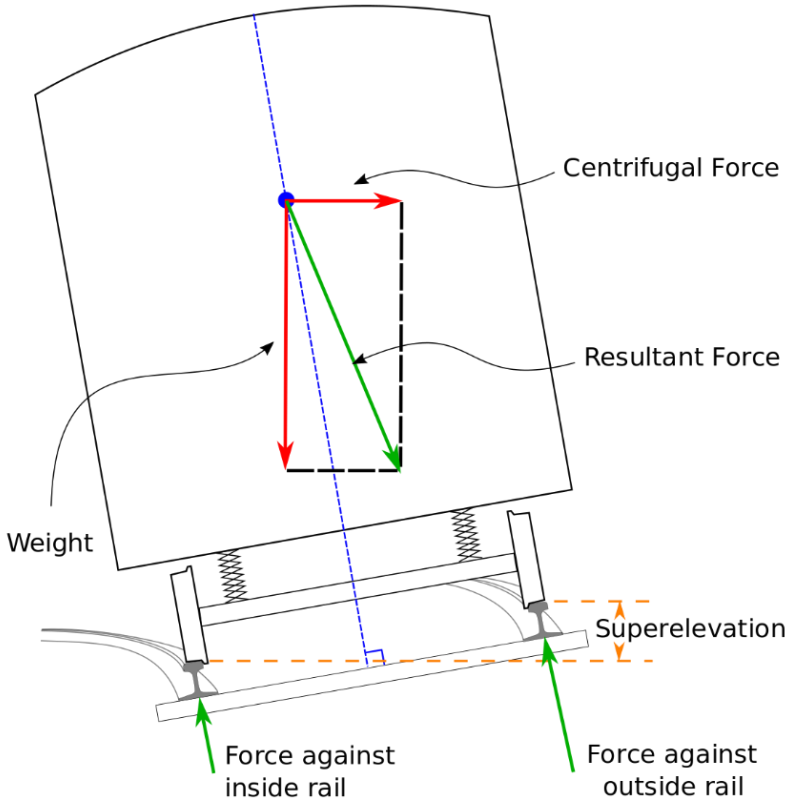

Figure 2.23 - Curved track superelevation [32]

In the static case, the results obtained showed a decrease in buckling temperatures on curved tracks, Figure 2.24. As the rail curvature rises, there is an almost exponential decrease in the temperatures, showing the high influence of the rail curvature parameter.

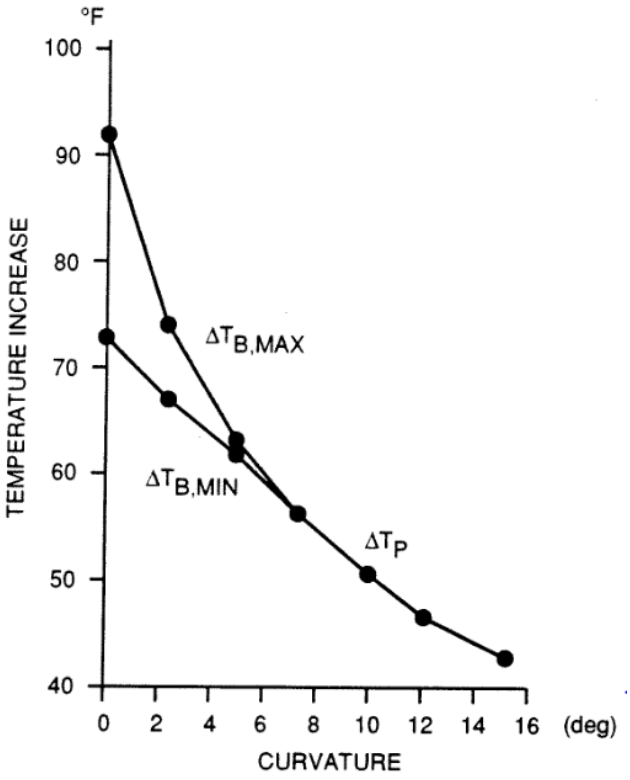

Figure 2.24 - Influence of rail curvature on buckling temperatures [17]

Additionally, the passage of trains introduces dynamic loads that further contribute to instability in the tracks. As a train moves through a curved section of rail, the carts exert a lateral force on the rails. Due to the centrifugal force produced by the train's momentum when it enters a curved segment, the outer rail is subject to an increased lateral load. These lateral forces are dependent on a series of variables when considering the dynamic case, such as the cart weight, speed, track curvature, and superelevation [22]. These factors need to be considered for determining the speed limits on rails to prevent track buckling to occur, especially when considering high-speed trains

3. Materials and Methodology

The methodology employed in this study is structured into four main parts: material properties, numerical model description, model validation, and a subsequent parametric study focused on rail buckling. Initially, the properties of steel rails, concrete, and wood sleepers are defined. Subsequently, the development of the numerical model is elucidated. In the third section, the numerical model developed and validated based on previous research results is validated. Lastly, the validated model is subjected to a parametric analysis aimed at comprehending the impact of individual parameters on buckling temperatures.

3.1. Material Properties

This section provides a comprehensive overview of the material properties employed for conducting thermal buckling simulations. Specifically, it includes the steel properties of the rail, as well as the properties of wood and concrete associated with the sleeper.

3.1.1. Rail Properties

In this specific model, the rail material used was R260 steel grade. To determine the stress-strain relationships at different temperatures, the Ramberg-Osgood model (equation 3.1) was utilized.

The constants (β and n) required for the model were determined by referring to the Kamaya study [33]. In equation 3.1 the strain and the stress values are represented by ε and σ. The elastic modulus is given by E and the yield stress by σ_0.

$$\varepsilon = \frac{\sigma}{E} + \beta \frac{\sigma 0}{E} \left(\frac{\sigma}{\sigma 0}\right)^n \tag{3.1}$$

Reduction factors have been applied to both the elastic modulus and yielding stress [34], enabling the establishment of the constitutive model. The stress-strain curve model is then compared with the engineering curve obtained from experimental data, see Figure 3.1 [35].

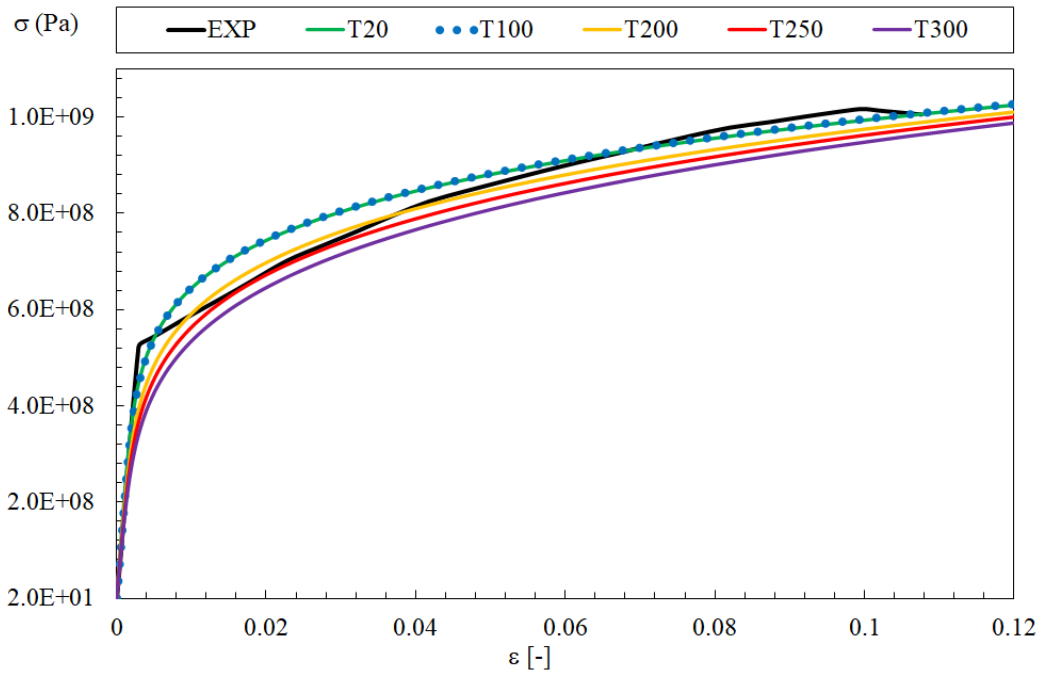

Figure 3.1 – Stress strain curve model at elevated temperatures.

Furthermore, it is necessary to define the thermal elongation of the material for different temperatures. Using equation 3.2, proposed by EN 1993-1-2 [34], the thermal elongation was calculated for temperatures of 20, 100, 200, and 300°C (T20, T100, T200, T250 and T300, in Figure 3.1). Subsequently, these values were inputted into the numerical model.

$$\frac{\Delta l}{l} = 1.2 \cdot 10^{-5} T + 0.4 \cdot 10^{-8} T^2 - 2.416 \cdot 10^{-4} \quad (3.2)$$

3.1.2. Sleeper Properties

The mechanical properties of concrete sleepers can exhibit significant variations depending on their class and porosity. In this study, concrete of class C20/25 was specifically chosen for investigation. According to the Eurocode 2 guidelines [36], this particular class of concrete demonstrates a modulus of elasticity of 30 GPa and a Poisson's ratio of 0.2. During the simulation process, it was assumed that the material behaved as a linear isotropic substance.

Regarding the mechanical properties of wood, the strength values can differ based on the wood type, species, and moisture content. In the context of railway sleeper construction in the United States, red oakwood is a commonly utilized wood species. Therefore, red oakwood was selected as the specific wood species for this research.

Since wood is an orthotropic material, its properties such as the modulus of elasticity, Poisson's ratio, and shear modulus vary based on the orientation of its fibers [37], as illustrated in Figure 3.2. These orthotropic relationships are presented in Table 3.1, with *E* representing the modulus of elasticity, *G* denoting the shear modulus, and μ representing Poisson's ratio. For this research,

considering the fiber orientation, the base values selected for E, μ, and G were 16 GPa, 0.3, and 1.2 GPa, respectively.

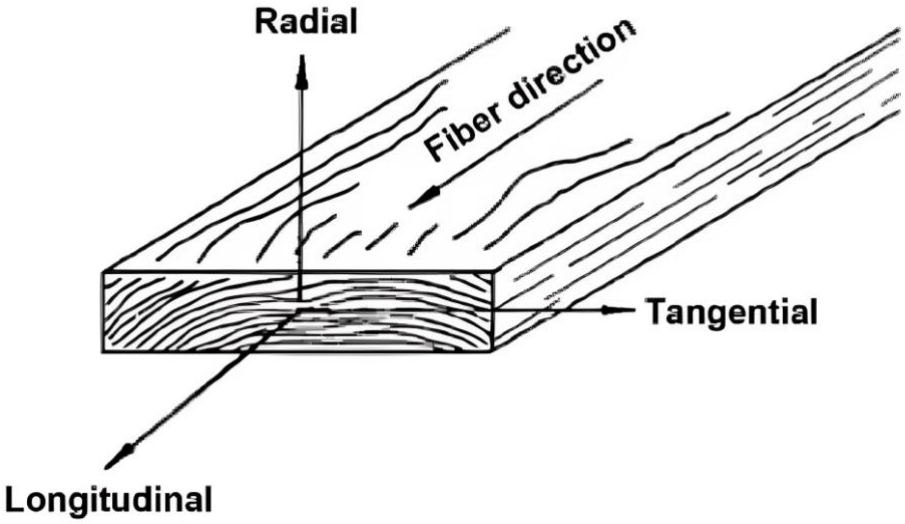

Figure 3.2 - Orthotropic wood axis representation [37]

Table 3.1 - Wood orthotropic relationships [37]

Specie	E_T/E_L	E_R/E_L	G_{LR}/E_L	G_{LT}/E_L	G_{RT}/E_L	μ_{LR}	μ_{LT}	μ_{RT}
Red Oak	0.082	0.154	0.089	0.081	-	0.35	0.448	0.56

3.2. Description of the model

To determine the safe operating temperature for different parameter sets a nonlinear finite element model was created. The model incorporated a GMNIA (Geometric Material nonlinear

Imperfection Analysis) model to represent the rails, sleepers, fasteners, and ballast. Ansys Mechanical ADPL was used to develop the finite element model of the railroad track. In the model, the main rail components, such as the rail and sleepers, were represented using Timoshenko 3D finite element beam BEAM188 models. These models had six degrees of freedom per node, cubic interpolating functions, and employed the full integration Gauss method.

To account for the lateral and longitudinal resistance of the ballast, nonlinear springs represented by the finite element COMBIN39 were used. This element is a 3D finite element unidirectional element that possesses nonlinear generalized force-deflection capability. It has variable stiffness in the longitudinal or torsional directions. For 3D applications, the longitudinal stiffness demonstrates uniaxial tension-compression behaviour with up to three degrees of freedom at each node (translations in space). In the case of torsional behaviour, it is purely rotational (with ROTZ rotational degree of freedom for the element). This element employs linear interpolating functions using exact integration.

The meshing for the BEAM188 elements was performed manually according to specific guidelines. Each rail element was assigned a length of 0.085 m, while the sleeper elements were modelled with a length of 0.11 m. Figure 3.3 illustrates the model meshing, which remains consistent for both tangent and curved models.

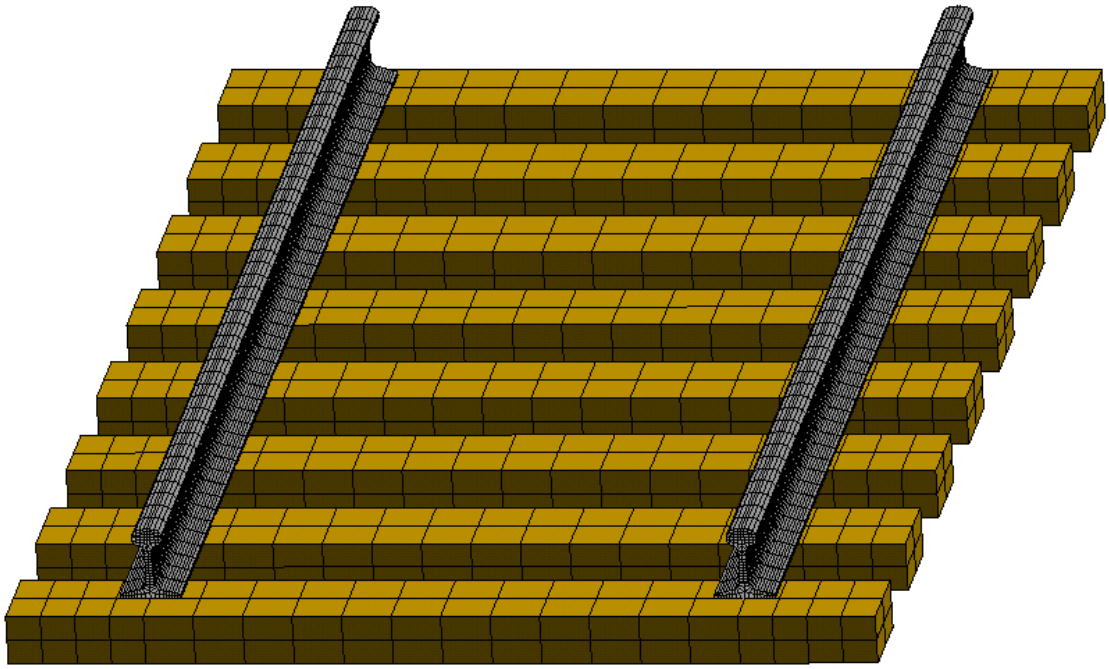

Figure 3.3 - Finite element model meshing (Only 8 sleepers)

Each sleeper in the model is associated with two lateral resistance elements, two longitudinal resistance elements, and two torsional resistance elements (not depicted in Figure 3.3). These elements collectively represent the resistance offered by the ballast-sleeper interaction in both the lateral and longitudinal directions.

The torsional resistance elements account for the impact of the fasteners that connect the rail to the sleeper, as illustrated in Figure 3.4. During the occurrence of the lateral deformed shape mode, one lateral resistance element experiences compression, signifying the highest level of resistance, while the other resistance element, operating in the same direction, is subjected to tension, representing the lowest level of resistance.

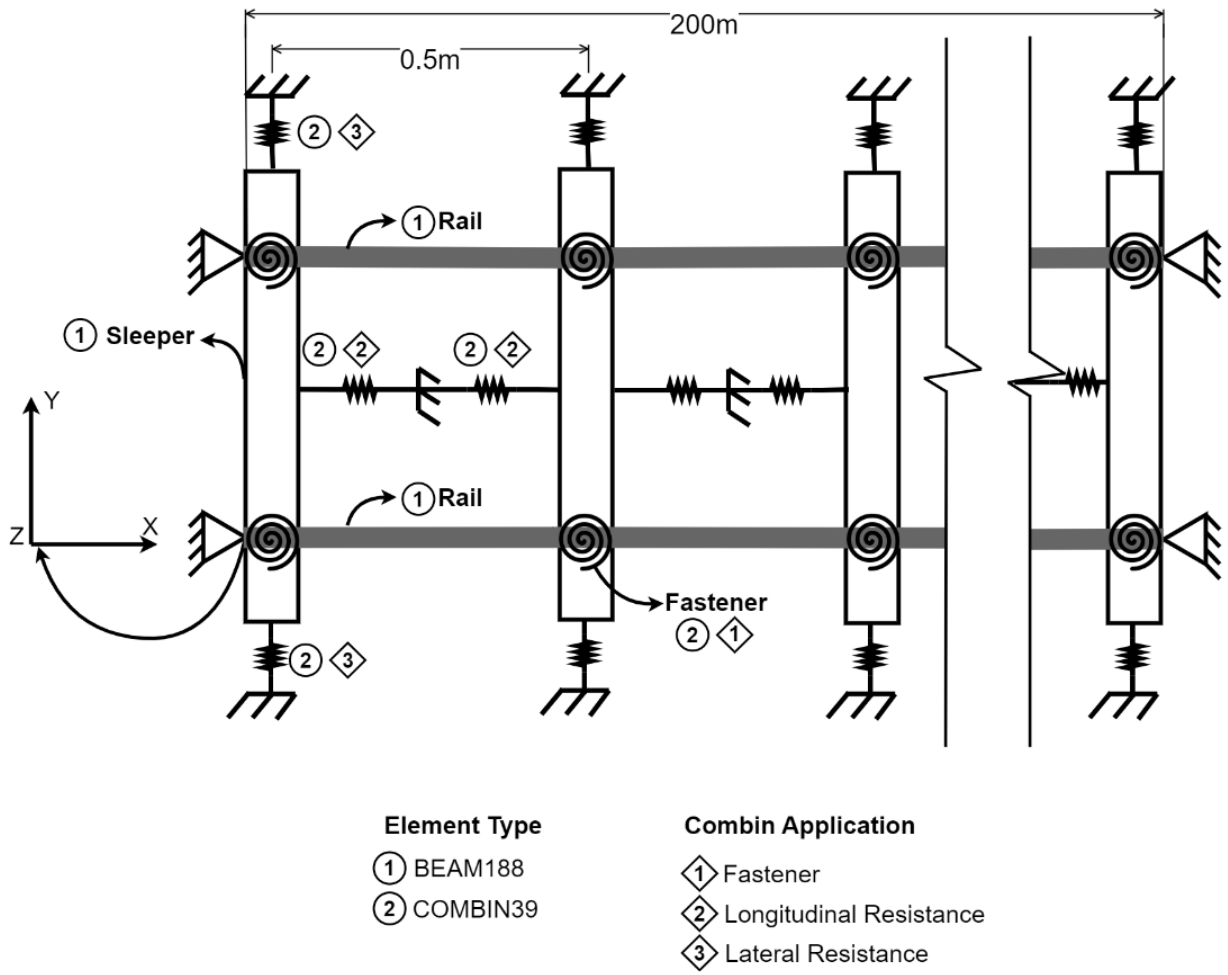

Figure 3.4 - Rail track model scheme.

Based on previous research [18], the stiffness of the fasteners can be approximated using a linear behaviour model employing COMBIN39 elements. Each COMBIN39 element in the model possesses distinct degrees of freedom, which are summarized in Table 3.2.

Table 3.2 – Option values for COMBIN39 finite elements.

Element Application	Degree of Freedom
Lateral Ballast Resistance	Translation in the Y axis
Longitudinal Ballast Resistance	Translation in the X axis
Fastener Torsional Resistance	Rotation in the Z axis

To connect the rail and sleeper nodes, a coupling restraint was incorporated, particularly at the position of the fasteners. This coupling restraint ensured that both nodes (sleeper node and rail node) had identical translations in the X, Y, and Z directions, as well as rotations in the X and Y directions. However, the rotation along the Z axis remained independent, enabling the modelling of the fastener connection between the sleeper and each rail.

Additionally, the translation along the Z-axis for all nodes was constrained, meaning there was no freedom of movement in that direction. Furthermore, the ends of the rails were restrained in all degrees of freedom, except for rotation around the Z axis.

3.3. Model Validation

To carry out the parametric study, the initial step involves validating the numerical model. In this study, the validation of the numerical model was accomplished through comparison with the previous work of Kish et al [18]. The authors examined the buckling phenomenon in both tangent and curved railways, considering a 200 m length rail, which was replicated in the software for analysis and evaluation. The primary focus of the validation process revolves around the

examination of buckling curves, which enable us to determine the temperatures at which buckling phenomena occur.

3.3.1. Validation Parameters

For tangent and curved tracks, an initial imperfection δ_0 with 41mm and 38mm amplitudes was applied to each model, respectively. These imperfections were applied in a central region, in the imperfection region of 11m in length, as illustrated in

Figure 3.5 and imposed in the experimental test.

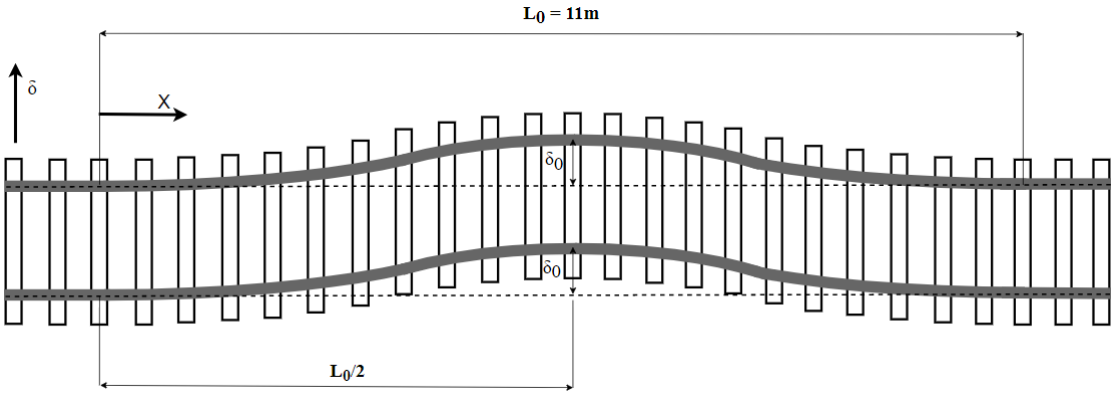

Figure 3.5 – Region for the Initial Imperfection of the rail track.

Additional parameters employed in the finite element model were also derived from experimental research and are provided in Table 3.3.

Table 3.3 - FE model parameters used for validation

Track Type	Track Radius [m]	Rail Profile	Sleeper Material	Rail Gauge [mm]	Initial Imperfection [mm]	Rail Length [m]
Tangent	-	132RE	Wood	1435	41 (L_0/268)	200
Curved	350	132RE	Wood	1435	38 (L_0/265)	200

The study employed as the foundation for validating the numerical model did not carry out measurement tests for lateral and longitudinal resistances. The solely available information indicates that the ballast underwent compaction after the introduction of the imperfection [18]. Because of that, values from previous experimental studies [14], [23], were used for the validation and applied for each corresponding COMBIN39 finite element.

The values employed for the purpose of validation are obtained through tests conducted on wooden sleepers and compacted ballast. The validation process includes the utilization of corresponding curves representing fastener torsional resistance, ballast lateral resistance, and ballast longitudinal resistance, as depicted in Figure 3.6, Figure 3.7, and Figure 3.8, respectively. Since its unknown the exact lateral resistance of the experimental study is, the peak value of the lateral resistance used for the validation was adjusted to increase the accuracy of the model. For the tangent rail configuration, the peak value of curve 2 reached 12.3 kN, and for the curved rail configuration, curve 3, reached 11.9 kN (Figure 3.7).

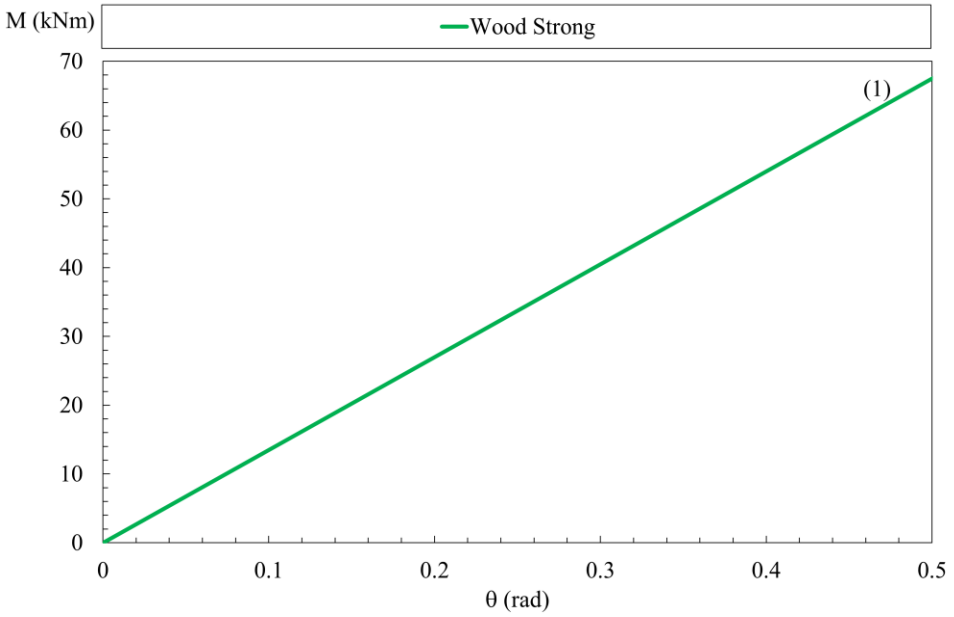

Figure 3.6 – Fasteners torsional stiffness (torsion moment versus rotation angle).

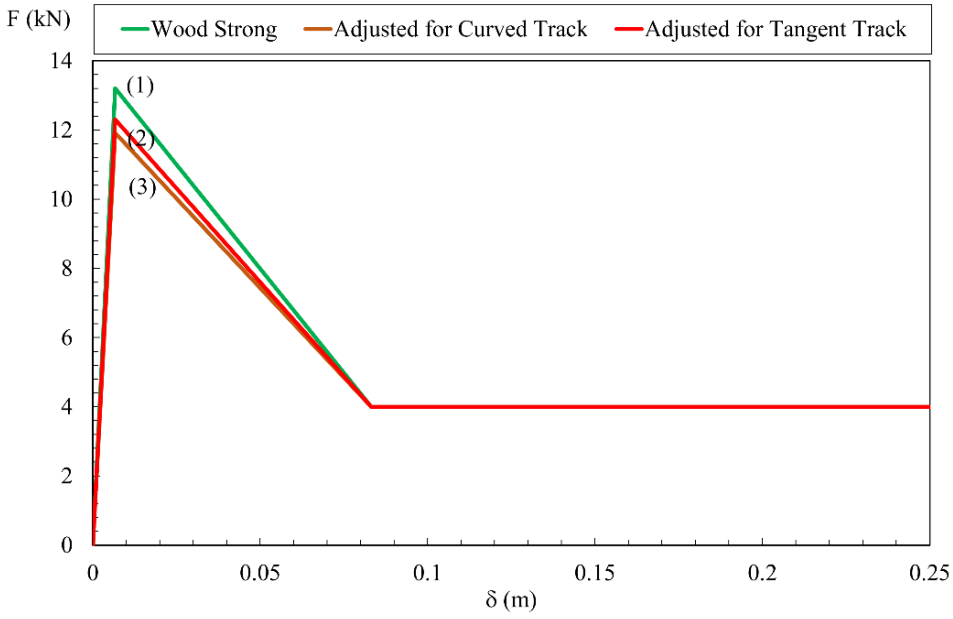

Figure 3.7 - Lateral resistance per sleeper (force versus displacement).

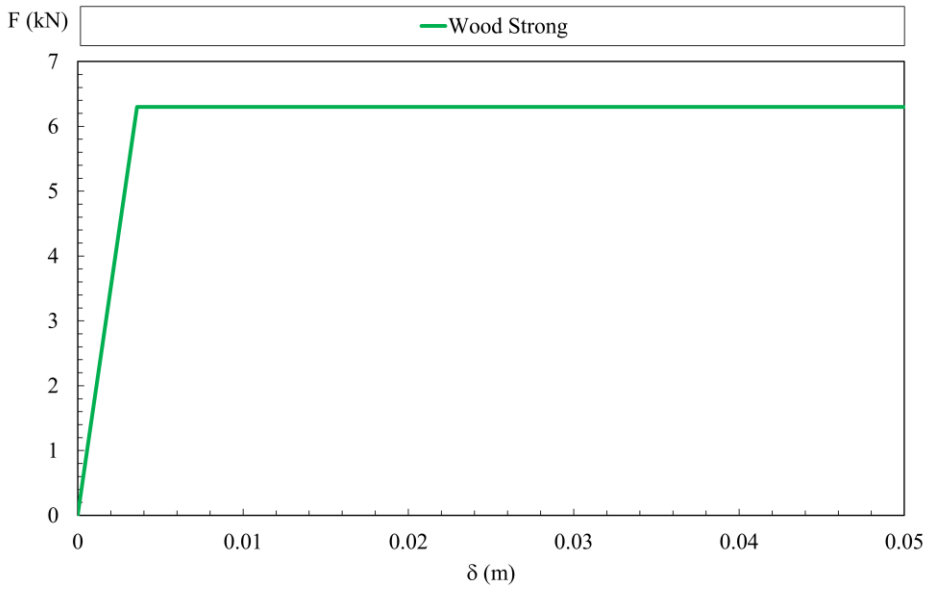

Figure 3.8 - Longitudinal resistance per sleeper (force versus displacement).

To examine the instability behaviour of the rail system, an incremental temperature was applied to all nodes of the rail structure. The process was initiated at an initial stress-free temperature of 22°C and gradually increased to 300°C. The stress-free temperature of 22°C selected for validation is the same as the one used in the experimental work upon which the validation is based. The analysis employed is known as GMNIA (Geometric Material Nonlinear Imperfection Analysis), which incorporates an incremental and iterative approach to determine the equilibrium position of the railway. The Newton-Raphson method is utilized during this analysis. The temperature increment is set at 4.6°C, with the possibility of reducing it to 0.0093°C. Convergence criteria are established based on internal loads, with a tolerance of 10^{-3} and a reference value of 1 N for force, a 10^{-3} tolerance and a reference value of 1 Nm for moment, and a tolerance of 10^{-2} and a reference value of 0.1 m for displacement. To enhance the convergence of the solution, a stabilization method incorporating an energy dissipation value of 10^{-6} was employed.

The rail profile used on the numerical model was the 132RE, the same as the experimental work. The ANSYS modulation was made based on the AREMA [12] specifications for each type of profile and the meshing were made manually. Additionally, the 136RE profile was also modelled, for later be used in parametric studies.

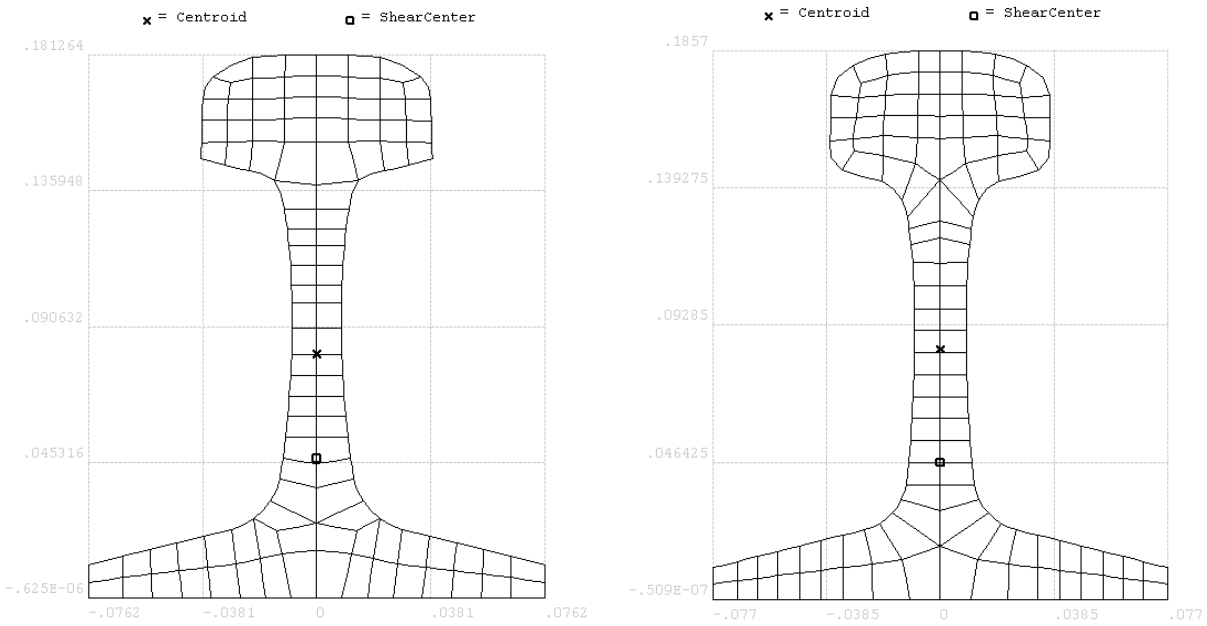

a)132RE b)136RE

Figure 3.9 – Meshed rail Profiles

3.3.2. Validation Results

After running the simulation, the result of the numerical simulation (NUM) was employed to ascertain the lateral displacement of the rail centre node, which was then compared to the

corresponding experimental results (EXP). This comparative analysis revealed the thermal buckling behaviour of the curved track, as illustrated in Figure 3.10.

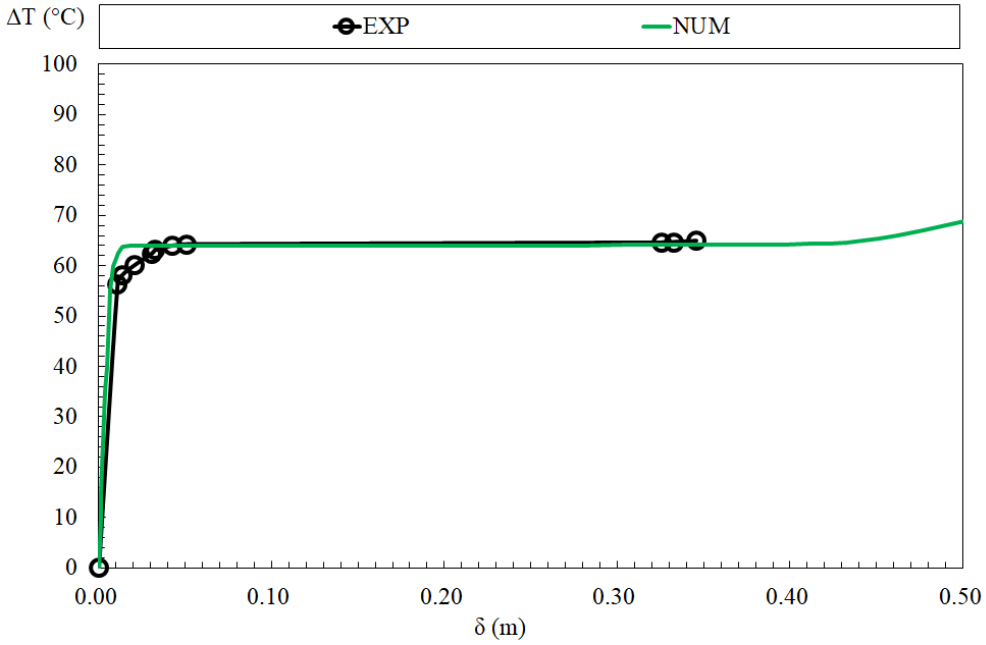

Figure 3.10 - Buckling curve for the curved track.

To calculate the error, the Root Mean Square Error (RMSE), as defined by equation 3.3, was utilized. Specifically, in the case of the curved track analysis, the RMSE was determined to be 2.9 ºC, considering multiple lateral displacement values. This value was determined based on 10 data points. It is worth noting that the highest error was observed in the first transition curve.

$$RMSE = \sqrt{\sum_{i=1}^{n} \frac{(\hat{y}_i - y_i)^2}{n}} \tag{3.3}$$

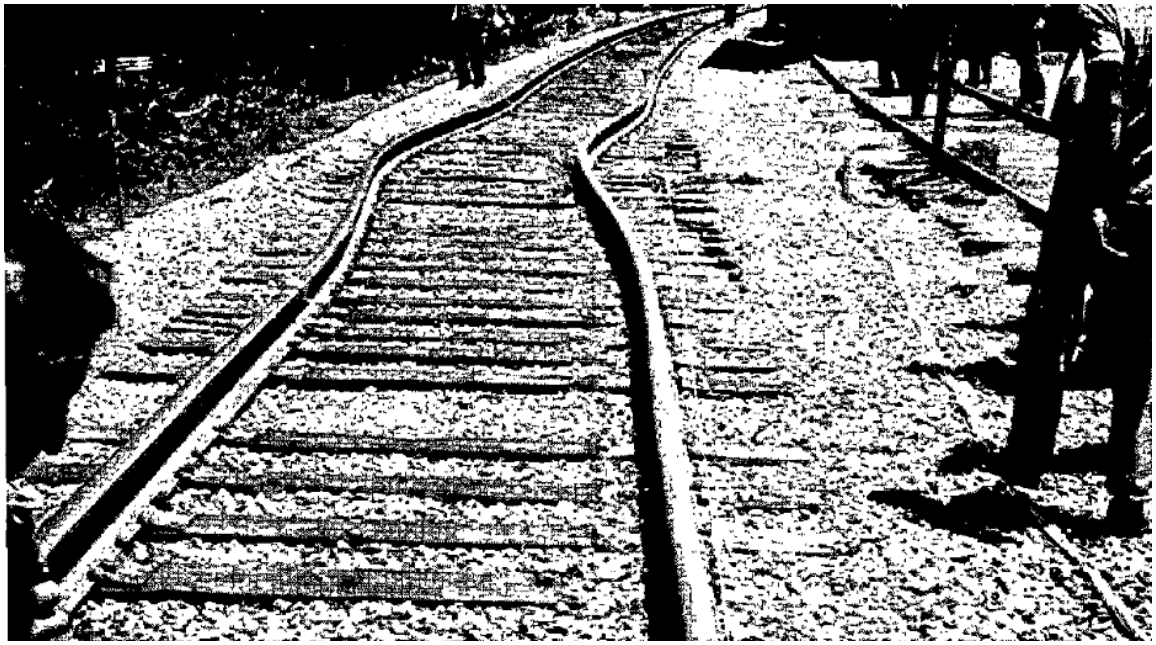

Figure 3.11 - Deformed buckling mode I for curved track [18].

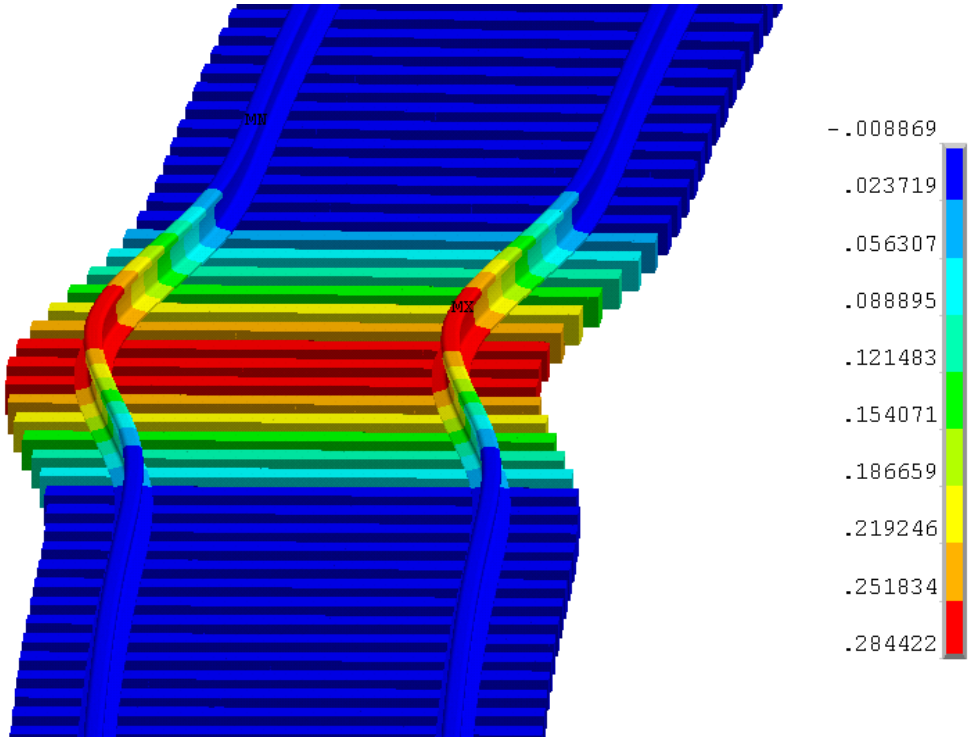

Figure 3.12 - Deformed buckling mode I for the curved track (numerical result).

Figure 3.11 illustrates the buckling mode shape observed in the curved track analysis, specifically buckling mode I. A significant lateral displacement is attained as the temperature increases by 64 ºC. Furthermore, the finite element method also produced a corresponding deformed buckling mode, along with its associated lateral displacement as demonstrated in Figure 3.12

In addition, the numerical simulations for the tangent track also involved comparing the lateral displacement of the central rail node with the corresponding experimental results. This comparative analysis is depicted in Figure 3.13. Notably, a higher buckling temperature of 80 ºC was determined for the tangent railway. The lateral displacement observed in the numerical simulation aligns remarkably well with the experimental measurements, indicating a strong agreement between them.

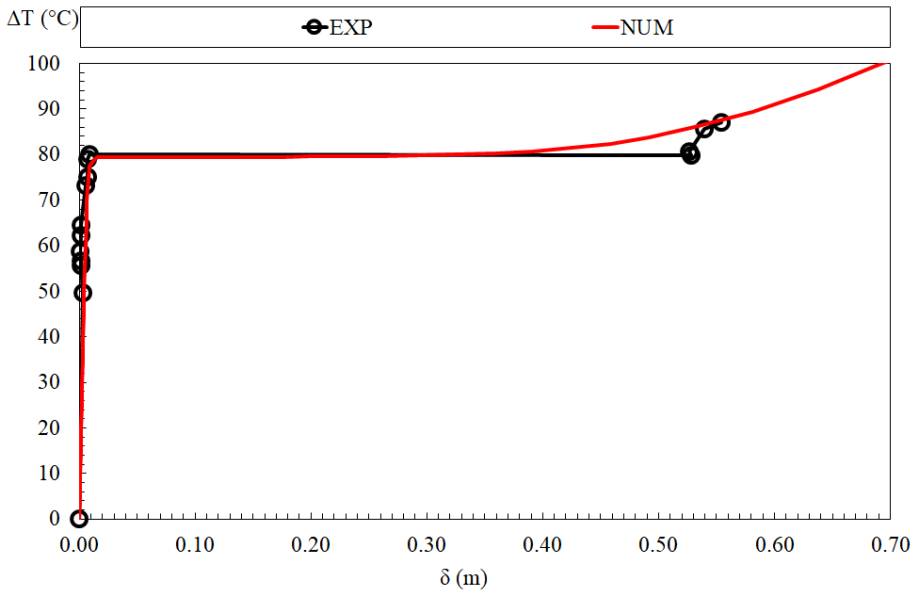

Figure 3.13 - Buckling curve for tangent track.

The deformed buckling mode of the tangent track has transitioned to mode III. However, it should be noted that the experimental deformed shape mode exhibits some degree of asymmetry [18]. According to the authors, the initial buckling mode was identified as mode I, primarily attributed to geometric imperfections. However, during the final stage, the mode shape transformed to mode III. This change in mode shape appears to be a common characteristic in tangent railways [18]. Figure 3.14 illustrates the buckling mode shape observed in the tangent track analysis, specifically mode III. A significant lateral displacement is obtained with an increase of 80 ºC in temperature. Furthermore, the finite element method produced a corresponding deformed buckling mode, although some of the curves didn't present the same amplitude as the experimental case as depicted in Figure 3.15.

The calculation of the Root Mean Square Error (RMSE) (according to Equation 3.3) for the tangent track analysis resulted in a value of 5.7 ºC. This value takes into account multiple lateral displacement values and is determined based on a dataset consisting of 9 data points. Notably, the highest RMSE value is observed in the second transition curve.

Figure 3.14 - Deformed buckling mode (III) to tangent railway track [18].

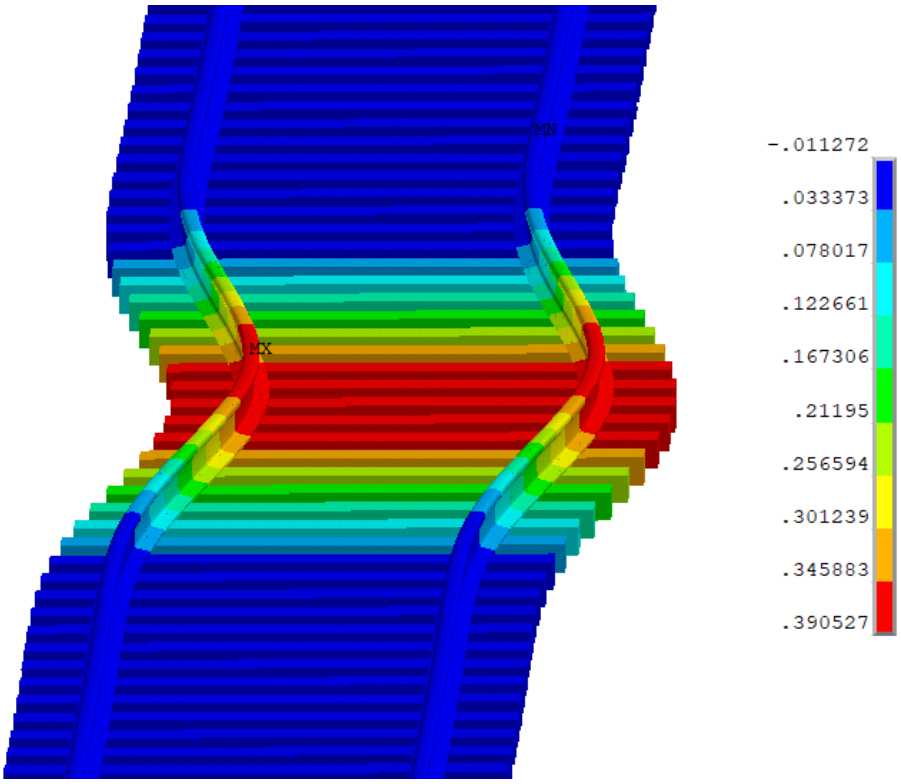

Figure 3.15 - Deformed buckling mode (III) to tangent railway track (numerical result).

3.4. Parametric Study

This chapter focuses on investigating the effects of key parameters on railway buckling behaviour. By altering and analyzing specific factors, insights can be gained to enhance the design and maintenance strategies of railway infrastructure. The parameters that have been varied in this study include track radius, initial imperfection, ballast resistance, rail profile and fastener torsional stiffness. They are shown in Table 3.4

Table 3.4 - Parameters used in simulations.

Track Radius [m]	**Initial Imperfection (*a*)**	**Sleeper Material**	**Ballast Resistance [N]**	**Rail Profile**	**Torsional Stiffness [Nm/rad]**
∞ (tangent) 350 m (curved)	*270* *500* *1000*	Concrete Wood	Strong Weak	136RE 132RE	Strong Weak

Regarding the track radius, the chosen values consisted of a tangent track and a curved rail. In both cases, the selected rail length was 200 meters and the curved track had a radius of 350 meters, see Figure 3.16. The primary objective of employing these parameters was to assess the disparity between straight and curved track segments and to identify which routes, necessitate enhanced caution. Notably, this study does not evaluate the impact of varying track radius.

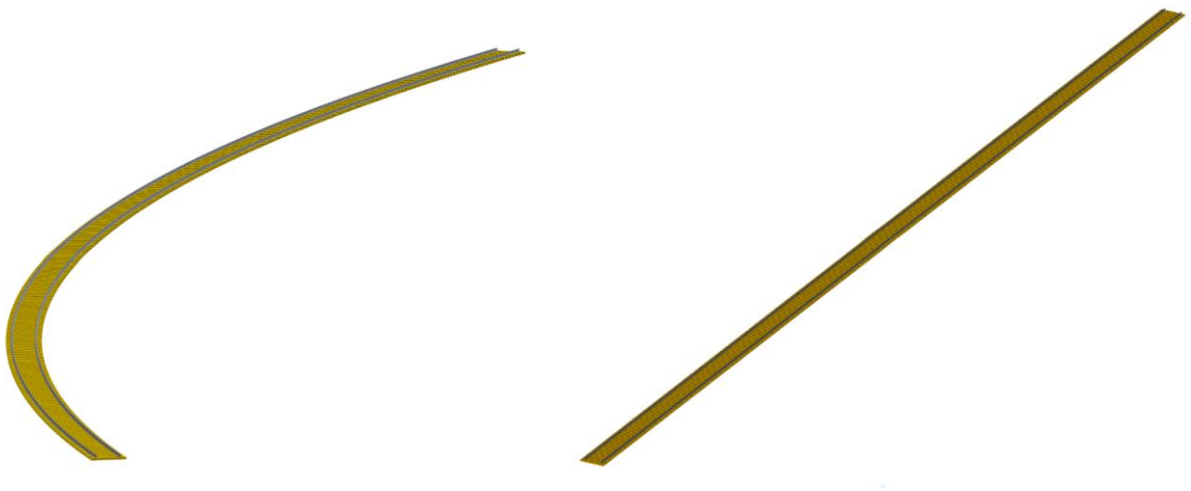

a) Curved Track b) Tangent Track

Figure 3.16 - Different track types

The misalignment was introduced at the central nodes of the rail length, with the amplitude δ0 being adjusted. The initial amplitude of the imperfection was determined by equation 3.4. The length of the imperfection, denoted as L_0, was maintained at a constant value of 11 meters, see Figure 3.5. The values for *a* started at 270 to align with the imperfections utilized during validation and were subsequently adjusted (See Table 3.4), ensuring that larger values corresponded to smaller imperfections. Also, the values for *x* start at 0 m and increase up to 11m (Maximum value for L_0).

$$\delta_0 = \frac{L_0}{a}\sin(\pi x / L_0) \tag{3.4}$$

The ballast resistance values used for COMBIN39 elements were obtained from reliable experimental studies. To simplify the numerical modelling and ensure an accurate representation

of the experimental values, the resistance applied by the ballast on the sleeper is categorized into two types: lateral resistance and longitudinal resistance. Also, this study not only includes a parametric analysis with strong and weak resistance values but also takes into account various sleeper materials, that influence both lateral and longitudinal resistances.

For the ballast lateral resistance, Zakeri's study [13] demonstrated a significant 28% increase in lateral resistance for concrete sleepers compared to wooden sleepers. Hence, this increase was considered in the simulation of concrete sleeper, based on the wood ballast lateral resistance curves [17], as shown in Figure 3.17.

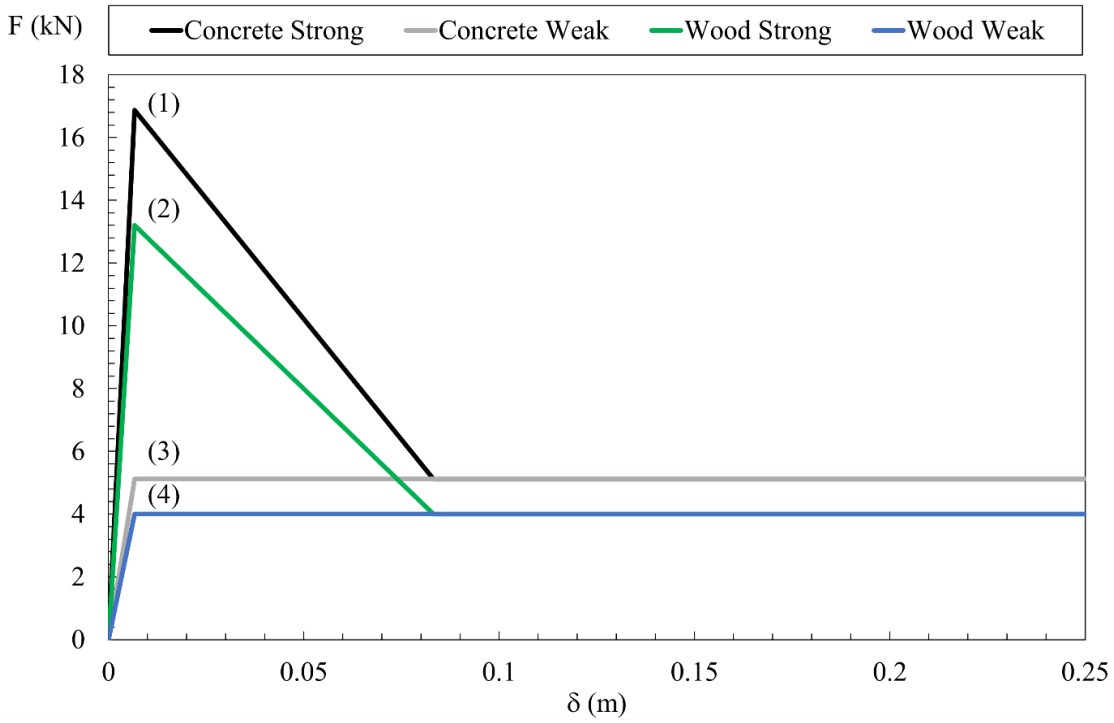

Figure 3.17 - Lateral resistance values for parametric study

Regarding the longitudinal resistance, nonlinear curves that effectively represent the ballast resistance were chosen based on Dersch's previous research [14]. These curves were linearized and are depicted in Figure 3.18. Considering that the longitudinal resistance is influenced by the material of the sleeper, this study examines four distinct curves. To assess the most critical scenarios, the strong ballast condition corresponds to fully compacted ballast with crib, while the values for the weak ballast condition were derived from experiments conducted with the no-crib condition.

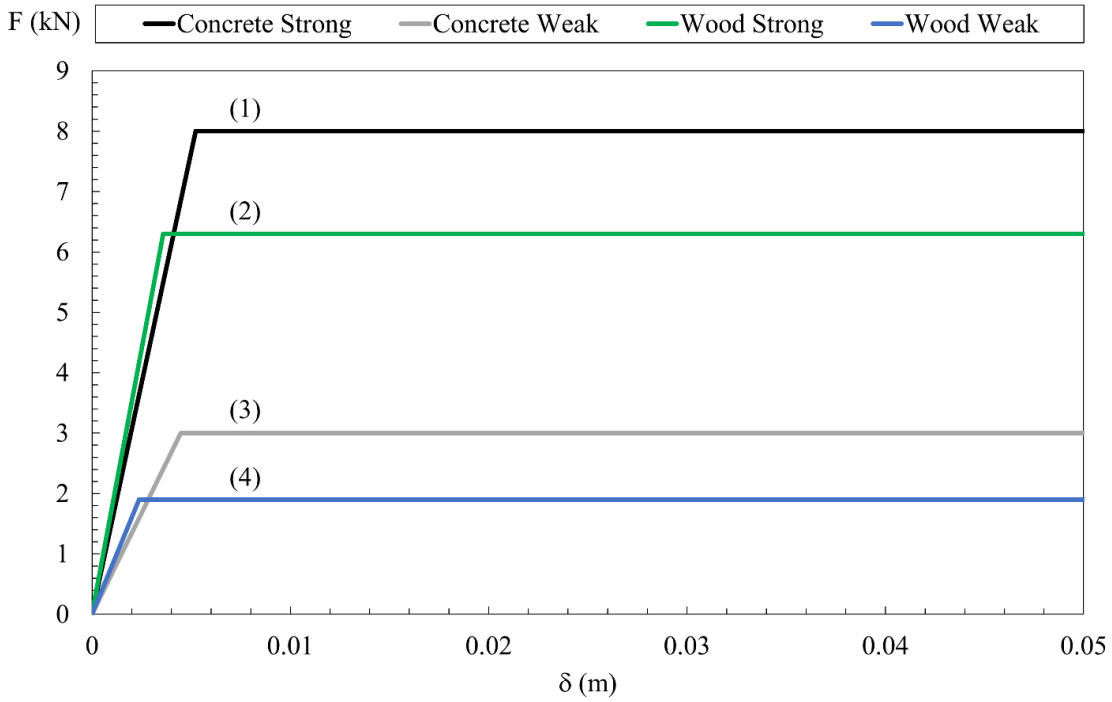

Figure 3.18 – Longitudinal resistance values for parametric study

It is important to note that a separate analysis of lateral and longitudinal resistance was not performed. Generally, the values chosen for simulations correspond to strong resistance (with

compacted ballast) and weak resistance (without compacted ballast). However, such an analysis is not meaningful when compared to the experimental case since both lateral and longitudinal resistances exhibit a similar level of compaction regardless of whether the ballast is compacted or not.

The simulations use different values for fasteners depending on whether they are used for concrete or wood sleepers. For concrete fasteners, the weak and strong values are based on the Pandrol and McKay fastener types respectively [17]. In contrast, for wooden sleepers, 4 spikes and 2 spikes were chosen as the fasteners. It's important to mention that all the fastener stiffness values used in this study were obtained from previous research [17] and were subjected to multi-linearization, as illustrated in Figure 3.19.

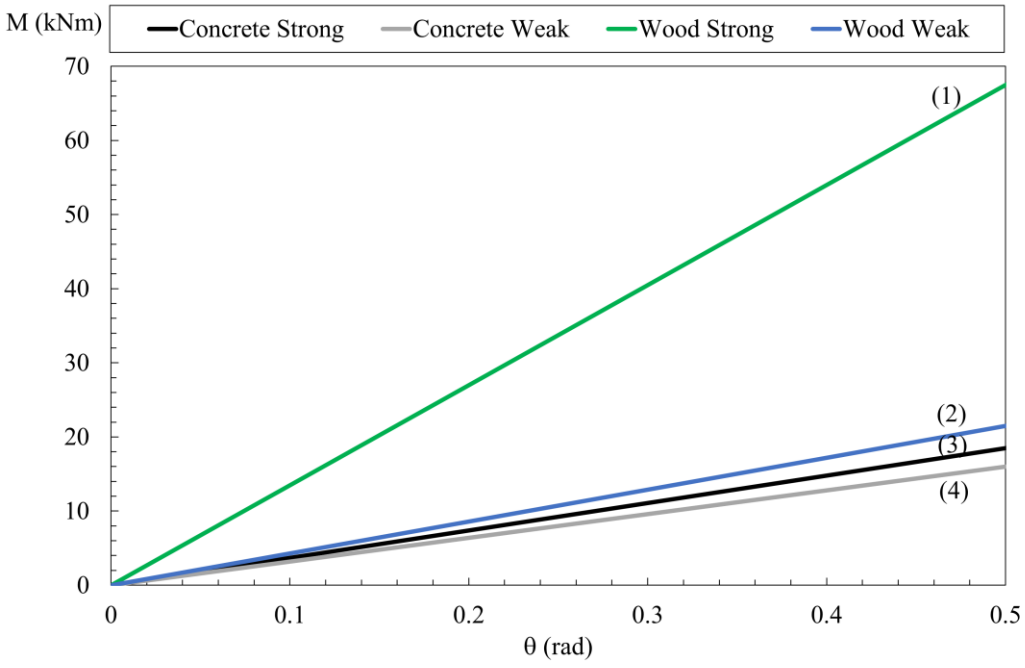

Figure 3.19 - Torsional stiffness values for parametric study

4. Results and discussion

The parametric analysis involved a total of 96 simulations, covering all possible combinations of the parameters. The average duration for simulations on tangent tracks was 45 minutes, while curved track simulations took an average of 25 minutes. The simulations were performed using hardware consisting of an Intel Xeon W-3365 processor with 8 cores and 32 GB of RAM.

Figure 4.1 - 4.6 present the buckling curves obtained from the parametric study. From the results, one can conclude that for both, curved and tangent railways, the concrete sleepers present higher buckling temperatures compared to the wood sleepers. The same happens for the track radius, where the tangent rails have always higher buckling temperatures when compared to curved rails. The 132RE rail profile generally presents a slightly higher buckling temperature than the 136RE rail profile.

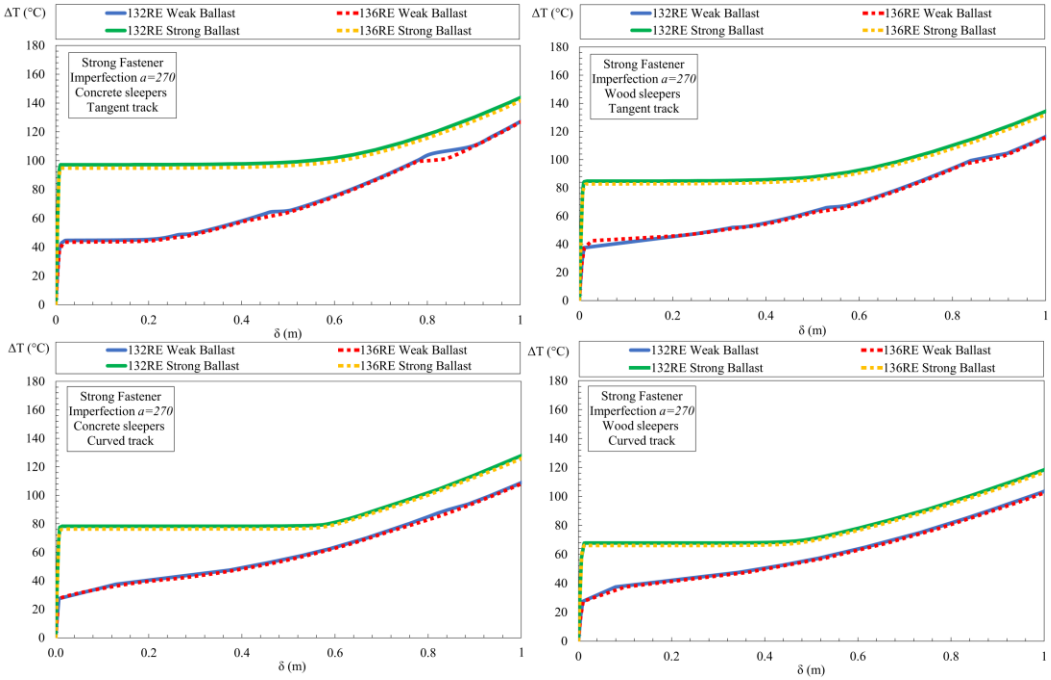

Figure 4.1 - Buckling curves for strong fastener and imperfection a=270.

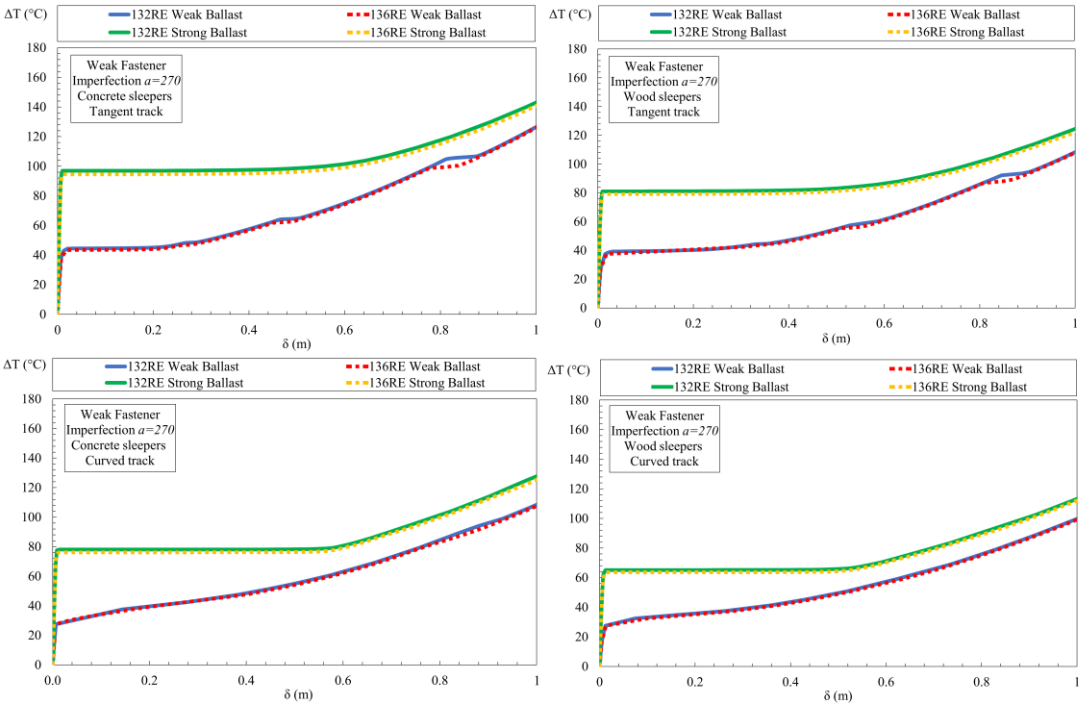

Figure 4.2 - Buckling curves for weak fastener and imperfection a=270.

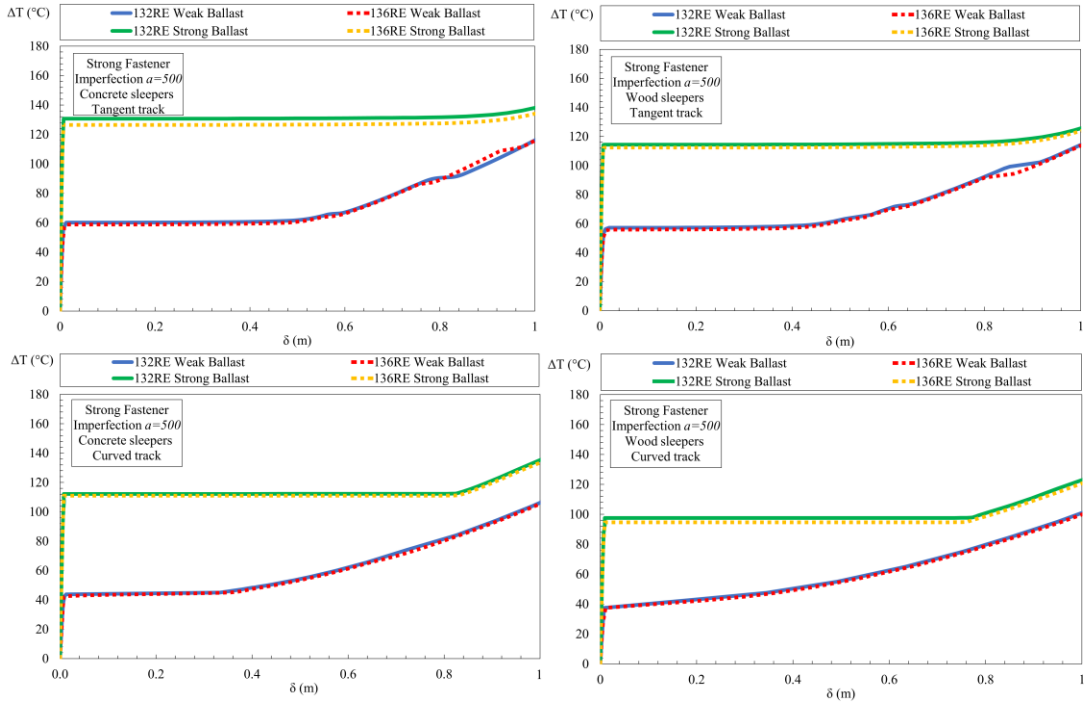

Figure 4.3 - Buckling curves for strong fastener and imperfection a=500.

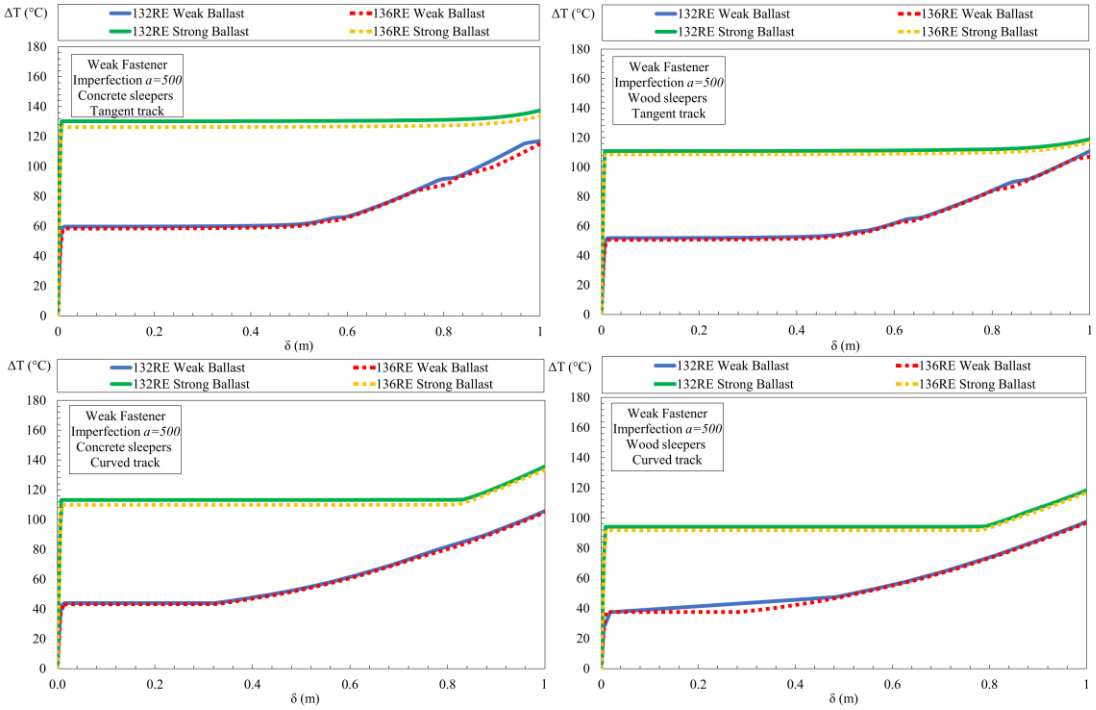

Figure 4.4 - Buckling curves for weak fastener and imperfection a=500.

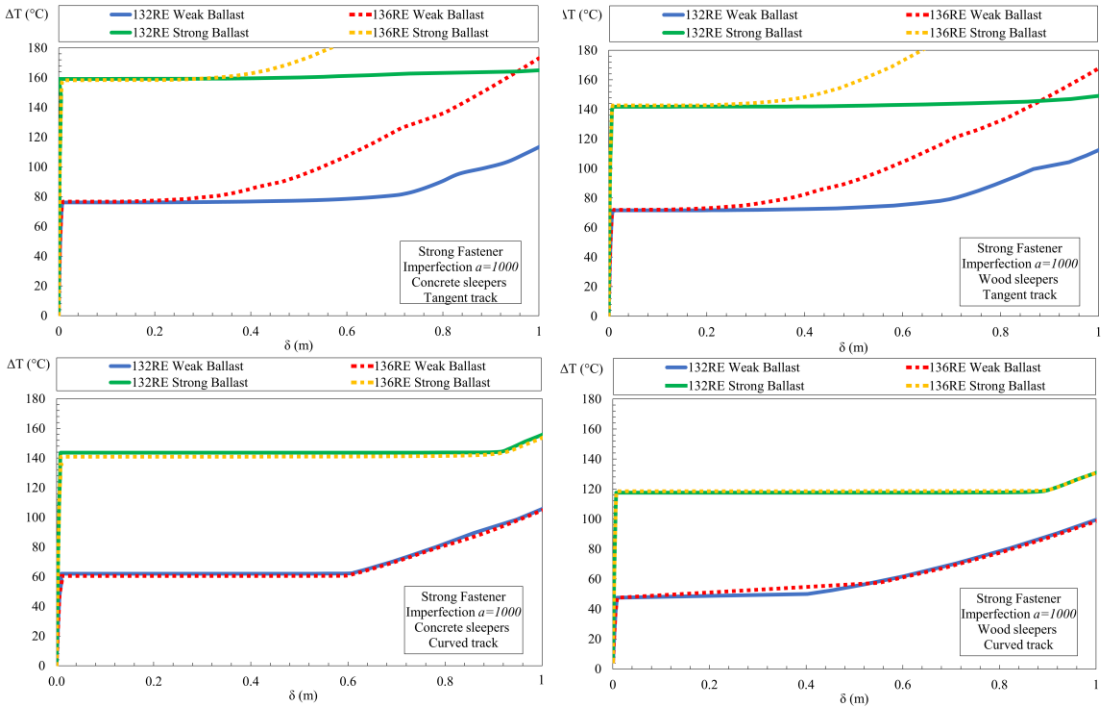

Figure 4.5 - Buckling curves for strong fastener and imperfection a=1000.

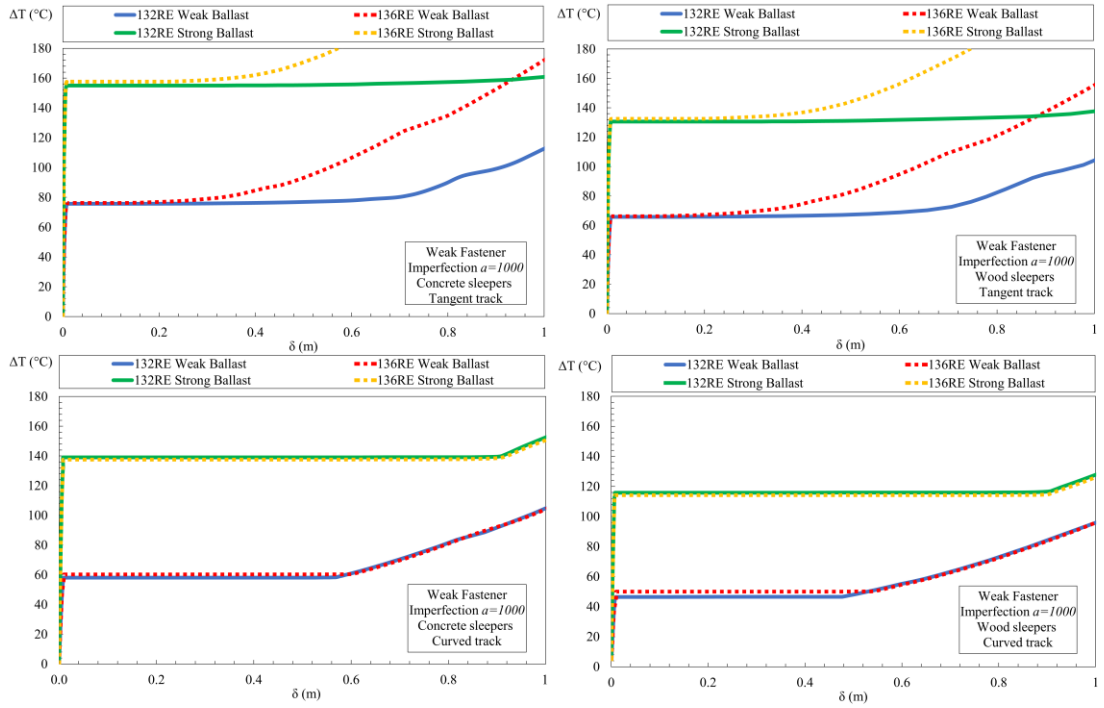

Figure 4.6 - Buckling curves for weak fastener and imperfection a=1000.

The results obtained from the analysis highlight that the primary factor in preventing rail buckling is the resistance provided by the ballast. Specifically, when considering concrete sleepers, a significant increase of 127% in rail buckling temperatures was observed when comparing strong ballast resistance values to weak resistance values. Similarly, for wood sleepers, an average increase of approximately 117% was observed across all simulations.

In the case of wood sleepers, the torsional stiffness values of the fasteners played a more significant role, resulting in a 6% increase in buckling temperatures for strong values compared to weak values. However, for concrete sleepers, this increase for strong values was only 1% compared to the weak alternative.

Regardless of the sleeper material, the utilization of the 132RE rail profile led to a 1% increase in rail buckling temperatures compared to the 136RE rail profile. Despite having a higher linear mass, the 136RE profile has a larger slenderness ratio, which promotes the occurrence of the buckling phenomenon.

Analyzing different track radii, it was observed that in tangent railways, the buckling temperatures were 18% higher compared to curved tracks in the case of concrete sleepers. Similarly, for simulations involving wood sleepers, a significant 20% increase in buckling temperatures was observed.

The influence of imperfections (represented by the a-coefficient) and track radius is depicted in Figure 4.7. Notably, imperfections have a greater influence on the temperature increase in cases with strong ballast. The results were categorized into four distinct groups based on ballast compaction and track radius. To establish safe operating temperatures for railways, a normal distribution analysis was conducted. This involved selecting the midpoint of each data and

subtracting twice the standard deviation. Using these adjusted points, a trend line was fitted to represent the safe operating temperature, encompassing 95% of the cases.

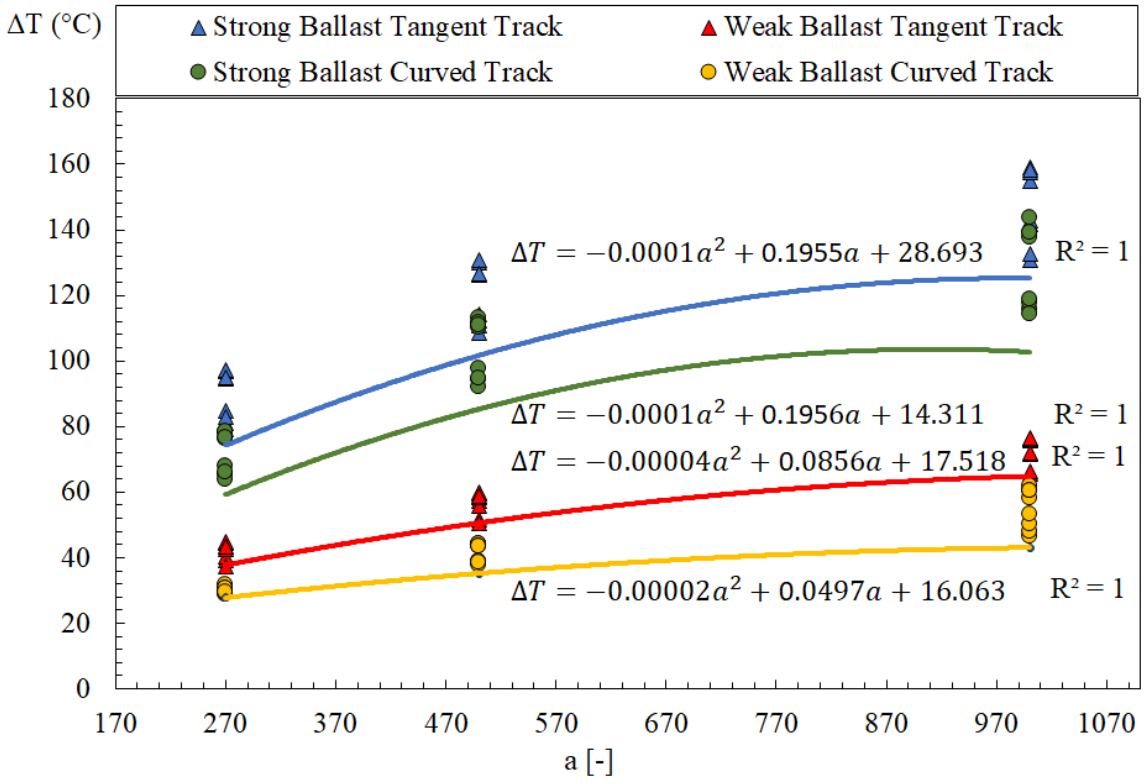

Figure 4.7 - Imperfection influence on buckling temperatures.

New proposals are presented as design curves, established for strong and weak ballast, and also for tangent and curved railways. The coefficient of determination R^2 is 1 for all the design formulas. Table 4.1 presents the buckling temperature increase compared to the imperfection *a=270*, taken as a reference.

Table 4.1 - Imperfection influence on buckling average temperatures.

Track Configuration	**Imperfection L_0**		
	a=270 (reference)	a=500 (variation)	a=1000 (variation)
Strong Ballast Tangent Track	89 ºC (-)	120 ºC (34%)	148 ºC (66%)
Strong Ballast Curved Track	71 ºC (-)	103 ºC (44%)	128 ºC (78%)
Weak Ballast Tangent Track	42 ºC (-)	57 ºC (35%)	73 ºC (72%)
Weak Ballast Curved Track	29 ºC (-)	41 ºC (38%)	55 ºC (87%)

The conducted parametric study has highlighted the significance of proper ballast maintenance, ensuring accurate and adequate compaction. Additionally, the proper alignment of the rails emerges as a critical factor in ensuring the safe operation of the railway. Furthermore, it can be deduced that the utilization of concrete sleepers enhances the railway's safety operation in terms of buckling, as it ensures higher buckling temperatures.

5. Conclusion

5.1. General Conclusions

The present study investigated the phenomenon of thermal buckling instability through the utilization of a three-dimensional numerical model. The model employed a three-dimensional finite element beam based on the Timoshenko hypothesis, along with a unidirectional element featuring nonlinear generalized force-deflection capabilities. To establish the credibility of the numerical model, experimental outcomes were compared, resulting in a favourable agreement characterized by a small root mean square error (RMSE). Subsequently, a parametric investigation was carried out to assess the pivotal parameters that influence rail buckling temperatures.

The research outcomes revealed that concrete sleepers exhibited a substantial 127% increase in buckling temperatures when comparing weak and strong ballast resistance. Similarly, wood sleepers experienced a 117% increase under the same conditions. Table 4 provides evidence that the initial imperfection exerted a notable influence on buckling temperatures across all track configurations. Concerning wood sleepers, the torsional stiffness of the fasteners played a significant role, leading to a 6% rise in buckling temperatures when comparing strong fastener stiffness to weak stiffness. In contrast, concrete sleepers demonstrated a mere 1% increase in buckling temperatures for strong fasteners compared to weak ones. Furthermore, both concrete and wood sleeper scenarios exhibited a 1% increase in buckling temperatures when utilizing the 132RE rail profile in comparison to the 136RE rail profile. Additionally, it was observed that

tangent tracks exhibited 18% higher buckling temperatures than curved tracks for concrete sleepers, while wood sleepers experienced a 20% increase.

Based on these findings, it can be conclusively determined that the primary factors contributing to the decrease in buckling temperatures are the condition of the ballast, track curvature, and initial misalignments of the track. These results underscore the critical significance of consistent track maintenance, appropriate ballast compaction, and the maintenance of proper track alignment for operational railway systems.

5.2. Future Works

The present study showed good correspondence with the experimental work used as a reference. However, the reference work did not specify the measurements of certain variables, such as the torsional resistance of the fasteners and the longitudinal and lateral resistance of the ballast. For future studies, it is suggested to conduct experimental tests in which these measurements are taken, and the corresponding values are inserted into the numerical model for better validation.

As a suggestion for new parameters that could be analyzed in the model, the inclusion of dynamic loads is proposed to understand how the passage of trains influences the buckling temperature. Additionally, the study of the influence of different curvature radii can also be conducted. For increasing the numerical model fidelity, the recommended superelevation values by standards for curved tracks can also be included.

6. Bibliography

[1] C. F. Bonnett, *Practical Railway Engineering*, 2nd ed. London: Imperial College Press, 2005.

[2] M. J. T. Lewis, "Railways in the Greek and Roman world," 2001.

[3] C. K. A. Mubarack and A. Upadhyay, "Stability of continuous welded rail on steel bridge subjected to thermal loading," *Structures*, vol. 34, pp. 4524-4524–4531, 2021, doi: 10.1016/j.istruc.2021.10.050.

[4] Y. Wu, P. Munro, M. G. Rasul, and M. K. Masud Khan, "A review on recent developments in rail temperature prediction for use in buckling studies," Wellington: Conference On Railway Engineering, Sep. 2010.

[5] "UIC safety report 2022 : significant accidents 2021," UIC, Paris, Oct. 2022.

[6] E. Manuel Cabrita, "Renovação de plataformas ferroviárias," Universidade do Porto, Porto, 2005.

[7] N. H. Lim, N. H. Park, and Y. J. Kang, "Stability of continuous welded rail track," *Comput Struct*, vol. 81, no. 22–23, pp. 2219–2236, Sep. 2003, doi: 10.1016/S0045-7949(03)00287-6.

[8] R. A. Smith, "Railways and materials: Synergetic progress," *Ironmaking and Steelmaking*, vol. 35, no. 7, pp. 505–513, Oct. 2008, doi: 10.1179/174328108X318888.

[9] A. Skarova, J. Harkness, M. Keillor, D. Milne, and W. Powrie, "Review of factors affecting stress-free temperature in the continuous welded rail track," *Energy Reports*, vol. 8, no. 107–113, pp. 107-107–113, 2022, doi: 10.1016/j.egyr.2022.11.151.

[10] A. V. N. Frigeri, M. C. Minhoto, P. A. G. Piloto, and D. A. Silva, "Thermal and Mechanical Behavior of Railway Tracks," Thesis, Instituto Politécnico de Bragança, Bragança, 2021.

[11] M. A. Van, "Stability of Continuous Welded Rail Track," Thesis, Delft University of Technology, 1997.

[12] "American Railway Engineering and Maintenance-of-way Association, Manual for Railway Engineering," USA, 2010.

[13] J. A. Zakeri and A. Bakhtiary, "Comparing lateral resistance to different types of sleeper in ballasted railway tracks," Tehran, 2014. [Online]. Available: www.scientiairanica.com

[14] M. S. Dersch, M. Potvin, A. de O. Lima, and J. R. Edwards, "Effect of Critical Factors Influencing Longitudinal Track Resistance Leveraging Laboratory Track Panel Pull Test Experimentation," *Transportation Research Record: Journal of the Transportation Research Board*, p. 036119812311554, Mar. 2023, doi: 10.1177/03611981231155420.

[15] V. A. Profillidis, *Railway Management and Engineering*, 4th ed., vol. 4. Farnnham, Surrey, England: Routledge, 2016.

[16] J. M. Sadeghi, J. A. Zakeri, and M. E. M. Najar, "Developing Track Ballast Characteristic Guideline In Order To Evaluate Its Performance," *International Journal of Railway*, vol. 9, no. 2, pp. 27–35, Dec. 2016, doi: 10.7782/ijr.2016.9.2.027.

[17] G. Samavedam, A. Kish, and J. Schoengart, "Parametric Analysis and Safety Concepts of CWR Track Buckling," Cambridge, MA, Dec. 1993.

[18] A. Kish, G. Samavedam, and D. Jeong, "Analysis of Thermal Buckling Tests on U.S. Railroads," Cambridge, MA, Nov. 1982.

[19] G. P. Pucillo, "Thermal buckling and post-buckling behaviour of continuous welded rail track," *Vehicle System Dynamics*, vol. 54, no. 12, pp. 1785–1807, Oct. 2016, doi: 10.1080/00423114.2016.1237665.

[20] G. P. Pucillo, "Train-induced load effects on the thermal track buckling," in *Joint Rail Conference*, Naples, Italy, Apr. 2019. [Online]. Available: https://proceedings.asmedigitalcollection.asme.org

[21] A. Miri, M. Dhanasekar, D. Thambiratnam, B. Weston, and T. H. T. Chan, "Analysis of buckling failure in continuously welded railway tracks," *Eng Fail Anal*, vol. 119, Jan. 2021, doi: 10.1016/j.engfailanal.2020.104989.

[22] A. Kish, G. Samavedam, and D. Jeong, "Influence of Vehicle Induced Loads on the Lateral Stability of CWR Track," Washington, Nov. 1985.

[23] Van. M.A., "Buckling analysis of continuous welded rail track," *HERON*, vol. 41, no. 3, pp. 175–186, 1996.

[24] N.-H. Lim, S.-Y. Han, T.-H. Han, and Y.-J. Kang, "Parametric Study on Stability of Continuous Welded Rail Track," *Steel Structures* , vol. 8, pp. 171–181, 2008.

[25] A. D. Kerr, "An analysis of thermal track buckling in the lateral plane," Princeton, NJ, Sep. 1976.

[26] I. N. Martínez, I. V. Sanchis, P. M. Fernández, and R. I. Franco, "Analytical model for predicting the buckling load of continuous welded rail tracks," *Proc Inst Mech Eng F J Rail Rapid Transit*, vol. 229, no. 5, pp. 542–552, Jul. 2015, doi: 10.1177/0954409713518039.

[27] V. Tvergaard and A. Needleman, "On localized thermal track buckling," *Int J Mech Sci*, vol. 23, no. 10, pp. 577-577–587, 1981, doi: 10.1016/0020-7403(81)90038-2.

[28] I. Villalba, R. Insa, P. Salvador, and P. Martinez, "Methodology for evaluating thermal track buckling in dual gauge tracks with continuous welded rail," *Proc Inst Mech Eng F J Rail Rapid Transit*, vol. 231, no. 3, pp. 269–279, Mar. 2017, doi: 10.1177/0954409715626957.

[29] A. V. N. Frigeri, M. Minhoto, P. A. G. Piloto, and D. A. Silva, "Rail temperatures models validated with experimental measurements," *Revista Mecânica Experimental*, vol. 34, pp. 57–64, 2022.

[30] J. Filipe, C. Vieira, D. E. Carvalho, D. Raimundo, and M. Delgado, “Estabilidade Estrutural da Via Ferroviária,” Universidade do Porto, Porto, 2010. [Online]. Available: http://www.fe.up.pt

[31] Andrew Kish and Gopal Samavedam, “Track Buckling Prevention: Theory, Safety Concepts, and Applications Track Systems Safety,” Cambridge, MA, Mar. 2013. [Online]. Available: www.fra.dot.gov.

[32] “Cant deficiency.” https://en.wikipedia.org/wiki/Cant_deficiency (accessed Apr. 26, 2023).

[33] M. Kamaya, “Ramberg-Osgood type stress-strain curve estimation using yield and ultimate strengths for failure assessments,” *International Journal of Pressure Vessels and Piping*, vol. 137, pp. 1–12, Aug. 2014, doi: 10.1016/j.ijpvp.2015.04.001.

[34] CEN, “EN 1993-1-2: Eurocode 3: Design of steel structures - Part 1-2: General rules - Structural fire design,” Brussels, 2005.

[35] J. T. Maximov, G. V. Duncheva, I. M. Amudjev, A. P. Anchev, and N. Ganev, “A new approach for pre-stressing of rail-end-bolt holes,” *Proc Inst Mech Eng C J Mech Eng Sci*, vol. 231, no. 12, pp. 2275–2283, Jun. 2017, doi: 10.1177/0954406216630003.

[36] CEN, “EN 1992-1-1 Eurocode 2: Design of concrete structures - Part 1-1: General rules and rules for buildings,” Brussels, 2005. [Online]. Available: www.ipq.pt

[37] R. H. Falk, *Wood Handbook, Wood as an Engineering Material*. United States Department of Agriculture Forest Service , 2010. [Online]. Available: www.fpl.fs.fed.us.